A close-up photograph of a metal drill bit. A significant portion of the bit's tip has been removed, revealing a jagged, fractured surface. The remaining part of the bit shows a distinct cross-hatched texture, characteristic of a metal cutting process. Several small, dark, teardrop-shaped droplets are visible on the surface of the bit, likely from a cutting fluid. The background is dark and out of focus.

Design of experiment to measure swab pressure and mitigation of swab pressure due to cone pop-out

resulting from tubular expansion during mono-diameter drilling
F.T.M. Holtkamp

Design of experiment to measure swab pressure and mitigation of swab pressure due to cone pop-out

resulting from tubular expansion during
mono-diameter drilling

by

F.T.M. Holtkamp

to obtain the degree of

Master of Science
in Offshore & Dredging Engineering

at the Delft University of Technology,
to be defended publicly on Monday August 29, 2016 at 2:00 PM.

Student number:	1518275	
Project duration:	November 9th, 2015 - August 29th, 2016	
Supervisor:	Prof. Dr. Ir. A. Metrikine,	TU Delft
Thesis committee:	Dr. Ir. K. N. van Dalen,	TU Delft
	Ir. J. S. Hoving,	TU Delft
	Dr. Ir. W. Assaad,	Shell
	Dr. Ir. H. R. Pasaribu,	Shell

This thesis is confidential and cannot be made public.

Abstract

The discovery of oil and gas reservoirs remains the most important factor in the oil and gas industry. Every year new reservoirs keep being discovered, but their accessibility is becoming more challenging. In order to make the deep and hard-to-reach reservoirs more economic or even technologically possible, oil companies are looking for improved ways to drill wells. The technique Shell developed is called Mono-diameter Drilling (MOD), which allows minimal diameter change along the casing lengths installed using the expansion process. This is in contrast to a telescopic design used in conventional drilling operations. MOD allows larger inner liner diameters in deeper wells, enabling higher flow rates per well in deeper areas. Such technology is necessary for wells that are too deep or hard-to-reach for current technologies.

During MOD expandable casings with a smaller diameter are run through the host pipe with an expansion cone underneath. At the aimed location of the new casing, the volume between casing and formation is cemented. Before the cement is cured the cone is pulled through the casing by the drill string operated from the rig, expanding the diameter. At the location of the bottom of the host pipe and top of the installed casing an overlap exists between the casing and the host pipe. During the expansion at the overlap the casing, host pipe, cement of previous section, and the formation need to be expanded by the cone. This requires an increase in expansion force from the tower on the rig, and simultaneously the drill string is stretched (further) elastically and potential energy is stored in the form of strain. When the cone reaches the end of the overlap the contact area delivering frictional resistance between cone and casing decreases and the friction on the cone reduces and a gradual acceleration due to strain in the drill string initiates. After the overlap no contact area is left and the cone undergoes an enormous increase in acceleration; this is referred to as the cone pop-out. During cone pop-out, a void is created by the displacement of the cone. In order to fill this void fluids flow from the top of the bottom hole (decompression of this region), flow through the clearance between cone and host pipe, and flow through the drill string. The decompression is initiated at the bottom of the cone and fluid interface and propagates as a negative pressure wave (swab pressure wave) down hole. This wave reflects at the bottom of the hole, increasing the swab pressure. When the pressure difference between the inside and outside of the installed casing becomes too large, the casing collapses. Swab pressures are therefore very dangerous and need to be taken into account in well design.

In this research, an experiment has been designed in order to validate existing numerical models that predict swab pressures. The experiment is designed to validate the effect of four factors: the force required to expand the casing, the clearance between the expansion cone and the host pipe, the geometry of the tail of the cone, and the fluid properties in the well. In addition, two opportunities to mitigate the swab pressure problem have been researched: flow ports in the drill string and sudden additional flow in the system. The flow ports show promising numerical behaviour. It is advised to perform the experiment to validate the earlier numerical models and implement the flow ports in the design of the drill string. In the 10.2"/10.0" (host pipe/expanded liner) configuration a short pressure peak larger than the collapse pressure remains, therefore researching the dynamics of the pipe collapse is advised.

Preface

This thesis report is the product of nine months research at the Shell Rijswijk office and the Delft University of Technology.

This project has given me deep insights in the role of research and development engineers and their impact on Shell's production efficiency and capabilities. It gave me the opportunity to learn about the research of a new phenomenon, the design of an experiment, and finally the numerical implementation of possible solutions to the problem. This project has been executed by Jan-Willem van Dongen, who started in April 2014, followed by Harm Tillema who took over in December the same year and in turn by me in November 2015. The input from my predecessors consisted of several numerical models and a proposal for an experiment design to validate those models. In the beginning, the focus was mainly on finishing the experiment design in time. This process made me aware of the iterative nature of designing an experiment and the difficulty of the phenomenon to be tested. Due to the time constraints in the beginning and the help of Harm, my learning curve was very steep. I owe it to the people in the Wells R&D team, who have tested me and asked a lot of my engineering capabilities during my research, for the progress I made in this phase of the project. The focus in the second phase of my research was on numerical modelling and the implementation of mitigation strategies. The research necessary to thoroughly understand the numerical modelling caused my progress to slow down for some time, but in the end showed me that persistence can make the difference. This phase has made me understand the use of numerical applications in order to test hypotheses.

First I will thank Karel van Dalen, my daily supervisor at the university. Our meetings have always given me motivation to thoroughly understand the phenomenon and dig deeper into the matter. Also our nice discussions have made me aware of the complexity of this research, but to prevent to discourage me, he showed me practical opportunities to solve several problems.

Second, I like to thank Wissam Assaad, who has been my daily supervisor at Shell, for his support and his critical views on my work. He has shown me during the weekly meetings that a thorough understanding makes a difference in the design of the experiment and the understanding of the phenomenon. Especially in the beginning he made me explain the problems to him in detail, making me understand the problems better. In the end, he challenged me on my ways of solving the issues numerically, which made me better support my reasoning.

Third, I thank Jan-Willem van Dongen, my predecessor in this research and the creator of the original numerical model, for his contribution and helping me understand the model architecture, which was very useful in implementing the flow ports. Also, he has motivated me in the last months in order to deliver a sound project within the remaining time.

A fourth word of thank goes out to Rihard Pasaribu who has shown me that the practical use of research and economical reason for research should not be forgotten. In our bi-monthly meetings he steered me to show the applicability of the findings in my research.

My fifth word of gratitude goes out to Andrei Metrikine for being my supervising professor. He has motivated me by his genuine interest in the project and his insights in the fundamental dynamic issues at hand. During the progress meetings he has shared his knowledge and creative awareness to come to new research possibilities.

*E.T.M. Holtkamp
Delft, August 2016*

Contents

Nomenclature	ix
List of Tables	xi
List of Figures	xiii
1 Introduction	1
1.1 Well design	1
1.1.1 Conventional well	1
1.1.2 Mono-diameter well	2
1.2 Cone pop-out	4
2 Project overview	5
2.1 Problem statement	5
2.2 Experiment	5
2.3 Swab pressure mitigation	6
2.4 Approach	6
3 Experiment set-up	7
3.1 Objective	7
3.2 Outline	7
3.2.1 Requirements	10
3.2.2 Constraints	10
3.2.3 Experiment execution	10
3.2.4 Force calculations	12
3.3 Design	15
3.3.1 Drill string	15
3.3.2 Cone	17
3.3.3 Pressure vessel	18
3.3.4 Actuator	19
3.3.5 Sensors	22
4 Swab pressure mitigation	23
4.1 Flow ports.	24
4.1.1 Coupling of the annulus and drill string systems.	25
4.1.2 Pressure losses due to ports	27
4.2 Additional flow	28
4.2.1 Implementation	28
4.2.2 Numerical implementation	28
5 Results	31
5.1 Flow ports.	31
5.1.1 Results	32
5.1.2 Sensitivity analyses	35
5.2 Additional flow	38
5.2.1 Results	38
5.3 Discussion	40
6 Conclusion and recommendations	41
6.1 Conclusion	41
6.2 Recommendations	42

Bibliography	43
A Experiment set-up	45
B Assembly and experiment plan	47
B.1 Assembly	48
B.2 shear pin change	52
B.3 Cone change	53
C FEA results by 4RealSim	55
D Derivation of Bernoulli's equation for unsteady flow	59

Nomenclature

List of symbols

Symbol	Units	Description
A_{ds}	m^2	Cross-sectional area of the drill string
A_{ann}	m^2	Cross-sectional area of the annulus
$A_{flowport}$	m^2	Cross-sectional area of the flow port
A_n	m^2	Cross-sectional area of the nozzle
A_3	m^2	Cross-sectional area of the bottom hole
A_{piston}	m^2	Surface area of the piston
$c_{annulus}$	ms^{-1}	Speed of sound in the annulus region
$c_{bottomhole}$	ms^{-1}	Speed of sound in the bottom hole region
c_{damper}	$N(sm^{-1})^2$	Squared damping coefficient
c_{ds}	ms^{-1}	Speed of sound through drill string
C_p	–	Specific heat ratio at constant pressure
C_v	–	Specific heat ratio at constant volume
d	ms^{-2}	Deceleration rate
D_{ds}	m	Diameter of the drill string
D_{ann}	m	Diameter of the annulus
$D_{flowport}$	m	Diameter of the flow port
E	Nm^{-2}	Young's modulus
E_{ds}	Nm^{-2}	Young's modulus of the drill string material
E_{damper}	J	Energy absorbed by the damper
$E_{frictionsprings}$	J	Energy absorbed by the friction springs
E_{Kin}	J	Kinetic energy
$E_{P,nitrogen}$	J	Potential energy of the pressurized nitrogen
F_{buckle}	N	Buckling force
F_{damper}	N	Force exerted by the damper
$F_{frictionsprings}$	N	Force exerted by the friction springs
$F_{P,nitrogen}$	N	Force exerted by the nitrogen pressure
$F_{P,nitrogen}^{average}$	N	Average force of the nitrogen pressure during deceleration
$F_{upwards}$	N	Resultant upwards force
F_{water}	N	Force exerted by the water pressure on the drill string area
g	ms^{-2}	Gravitational acceleration constant
h	m	Height of the nitrogen chamber
I	m^4	Second moment of area
K	Nm^{-2}	Bulk modulus
K_{ann}	–	Loss coefficient for flow from the annulus into the flow port
K_{ds}	–	Loss coefficient for flow from the flow port into the drill string
K_{SC}	–	Loss coefficient for sudden contraction
K_{SE}	–	Loss coefficient for sudden expansion
k_{spring}	Nm^{-1}	Spring coefficient of one ring
k_{spring}	Nm^{-1}	Spring coefficient
$L_{annulus}$	m	Length of the annulus
$L_{bottomhole}$	m	Length of the bottom hole
L_{buckle}	m	Buckling length
L_{ds}	m	Length of the drill string
M_{piston}	kg	Mass of the piston
M_{system}	kg	Mass of the system
p	Nm^{-2}	Pressure

Symbol	Units	Description
p_3	Nm^{-2}	Pressure in the bottom hole area
P_{nitrogen}	Nm^{-2}	Pressure of the nitrogen in the actuator
P_{water}	Nm^{-2}	Pressure of the water in the pressure
P_{swab}	Nm^{-2}	Swab pressure
Q_{af}	m^3s^{-1}	Added flow
$s_{\text{deceleration}}$	m	stroke of deceleration
t	s	Time
Δt	s	Time step
u	m	Displacement
\underline{v}	3x1 vector	vector field equal to the gradient of the velocity potential
v_1	ms^{-2}	Velocity on node 1
v_n	ms^{-2}	Velocity in the nozzle
v_{avg}	ms^{-2}	Average velocity
V_{cone}	m^3	Volume of the cone
V_{ds}	m^3	Volume of the drill string
$V_{ds,i}$	m^3	Volume of the inner drill string
v_{flowport}	ms^{-2}	Velocity in the flow port (on node 4)
v_{piston}	ms^{-2}	Velocity of the piston
V_{nitrogen}	m^3	Volume of the nitrogen chamber
v_z	ms^{-1}	Velocity in the z-direction

Greek

Symbol	Units	Description
γ	–	Specific heat ratio
∇	m^{-1}	gradient of the vector field
ϕ	m^2s^{-1}	Velocity potential
ρ	kgm^{-3}	Density
ρ_w	kgm^{-3}	Water density
ρ_s	kgm^{-3}	Steel density

List of abbreviations

1D	One-dimensional
3D	Three-dimensional
API	American Petroleum Institute
CFD	Computational Fluid Dynamics
FEA	Finite Element Analysis
FSI	Fluid-Structure Interaction
FVM	Finite Volume Method
HSSE	Health, Safety, Security & Environment
ID	Inner diameter
MoC	Method of Characteristics
MOD	Mono-diameter Drilling
OD	Outer diameter
SPTR	Shell Projects & Technology Rijswijk
TAaP	Top Anchor and Pull
UTS	Ultimate Tensile Strength

List of Tables

3.1	Components of the experiment with their most important functions	9
3.2	Load cases of the experiment	11
3.3	Relevant parameters in actuator design	13
3.4	Relevant parameters in drill string design	13
3.5	Gas pressures and pressure forces for each stage of the experiment	13
3.6	Values for calculation of the potential energy of the pressurized nitrogen	14
3.7	Values for calculation of the kinetic energy in the system	14
3.8	Values for calculation of the energy taken up by the damper	14
3.9	Overview of tensile- and compressive forces	15
3.10	Maximum unsupported length in experiment per load case	17
3.11	Dimensioning of the pressure vessel	19
3.12	Characteristics of the 16600 Ringfeder friction spring	22
5.1	Base case settings for the flow port implementation	31
5.2	Values of parameters used in sensitivity analysis for flow ports	35
5.3	Area ratios for the pressure loss factor	35
5.4	Influence of the pressure loss coefficient on the swab pressure	37
5.5	Base case settings for the additional flow implementation	38
5.6	Values of parameters used in sensitivity analysis for additional flow	38
B.1	Design of experiment	47
C.1	FEA input variables	56

List of Figures

1.1	Cross-sectional view of conventionally drilled well	1
1.2	Installation of casing using MOD: (a) old casing is cemented in place, (b) new casing with cone and top anchor are run through the previously installed casing, (c) cone is pulled through new casing to expand the diameter and top anchor prevents casing to be pulled upward, and (d) new casing is installed with minimal change in diameter	2
1.3	Cross-sectional view of an MOD well	2
1.4	Expansion of casing at the overlap	3
1.5	Fluid flows during pop-out	4
2.1	The flow ports as suggested by Van Dongen.	6
3.1	The experiment set-up	8
3.2	Schematic drawing of the actuation and deceleration mechanism.	11
3.3	Free body diagram of the compressive and tensile loads during the experiment	12
3.4	FEA results from a 36.8 metric tonnes tensile load, performed by Callidus Group.	16
3.5	Design of the centralizers	17
3.6	The original cone (left) and the cone with extended tail (right)	18
3.7	The normal cone used in the experiment (left) and with extended tail (right)	18
3.8	Schematic drawing of the actuator.	19
3.9	The old titanium-printed piston design (left) and the steel machinable piston (right).	20
3.10	The current shear pin design.	21
3.11	The shear pin verification performed by Callidus (left) and Shell (right).	21
4.1	Flowrates below the cone in the normal model (left) and the model with gradual decrease of expansion force (right)	23
4.2	Pressure wave propagation after pop-out, the pressure waves propagating	24
4.3	Pressure wave propagation after pop-out and the flow that is induced by the pressure difference between the annulus (outer) and inner drill string (black arrows represent the flow direction)	25
4.4	Overview of the nodes that are recalculated using the flow port boundary conditions.	25
4.5	Flow port flow as coupled branched flow	26
4.6	Sudden contraction (a) and sudden expansion (b) in a pipe	27
4.7	The effective diameters for calculation of the loss factors due to expansion and contraction	27
5.1	Flow rates without (left) and with (right) flow ports.	32
5.2	Flow rates without (left) and with (right) flow ports with a gradual decrease in expansion force.	32
5.3	Pressure at the bottom without (left) and with (right) flow ports. The 150 bar line represents the 150 bar swab pressure that may not be exceeded.	33
5.4	Pressure without (left) and with (right) flow ports with a gradual decrease in expansion force.	33
5.5	Pressure without (left) and with (right) flow ports.	34
5.6	Pressure halfway the bottom hole without (left) and with (right) flow ports with a gradual decrease in expansion force.	34
5.7	Tornado charts of parametric study of flow ports for steady-state pressure.	35
5.8	The pressure at the bottom hole and halfway the bottom hole region, and the velocity in the flow ports for the far placement of the flow ports.	36
5.9	The effect of the diameter change of the flow ports for the normal model (left) and the model with gradual decrease of expansion force (right).	37
5.10	Sensitivity of the pressure loss coefficient, k , for the normal model (left) and the model with gradual decrease of expansion force (right).	37

5.11 Pressures at the bottom of the hole (left) and halfway the bottom hole (right) for different durations (up), flow rates (middle), and threshold pressures (bottom).	39
5.12 Effect of flow rate on the magnitude of the initial pressure wave.	40
A.1 Dimensions of the actuator (left) and full set-up (right)	45
B.1 Assembly step 1,2,3	48
B.2 Assembly step 4,5,6	49
B.3 Assembly step 7,8,9	50
B.4 Assembly step 10,11,12	51
B.5 shear pin change step 1,2,3	52
B.6 Cone change step 1,2,3	53
B.7 Cone change step 4,5,6	54
C.1 Schematic overview of the FEA input	56
C.2 Axial stresses at release (left) and until the bulge hits the spring (right)	57
C.3 Displacements of the cone, spring and top of the drill string during stroke of interest (left) and including deceleration of the system (right)	57
C.4 Displacements of the cone, spring and top of the drill string during stroke of interest (left) and including deceleration of the system (right)	57
C.5 Piston displacement and pressure in vessel (left) and the clearance between bulge and friction spring (right)	57
C.6 Forces in the damper, spring and nitrogen vessel	57

Introduction

This chapter introduces two important drilling technologies.

1.1. Well design

In the oil and gas industry, well drilling is an important part of the process of resource extraction. The final inner liner diameter influences the maximum production and in turn the economics of the well. An oil or gas well can reach depths of over 12 kilometres [1] [2]. In deep wells, different formation layers may be encountered, which have specific soil properties that define the strength of that layer. A well is drilled continuously for a certain length until either the drilling mud cannot provide enough support to prevent the walls to collapse, or a change in formation is encountered; the latter also includes depleted zones of reservoirs. When either occurs a new casing section is run into the borehole through the previous installed sections, before drilling continues. The manner in which the new casing section is installed down-hole is the major difference between conventional wells and mono-diameter wells.

1.1.1. Conventional well

Conventionally, a new casing section with a smaller diameter will be run into the borehole and cemented in place. Each new casing section reduces the well diameter significantly and leaves a smaller diameter for the final inner liner, as shown in figure 1.1 [3].

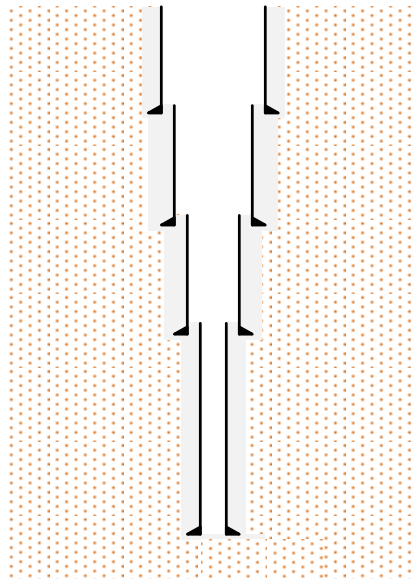


Figure 1.1: Cross-sectional view of conventionally drilled well

1.1.2. Mono-diameter well

Mono-diameter drilling (MOD) uses the technique of pipe expansion to maintain a single liner diameter along the length where MOD is applied. During MOD, a casing section is run into the hole and liquid cement is pumped between the casing and the formation; the cement cures over time. This first casing section is referred to as the host pipe. Then, an expandable casing section with a smaller diameter is run into the borehole and cemented in place. The casing is inserted with an expansion cone underneath, and before the cement of this section cures, the diameter is expanded by pulling the cone through the casing. The casing and the host pipe have an overlap section where the casing, the host pipe, the cured cement, and the formation need to be expanded by the cone. The expanded casing will have the same diameter of the previously installed casing, see figure 1.2 [4]. During the expansion process, the casing is held in place by an anchor placed on top and therefore this system is appropriately named the Top Anchor and Pull system (TAaP) [5].

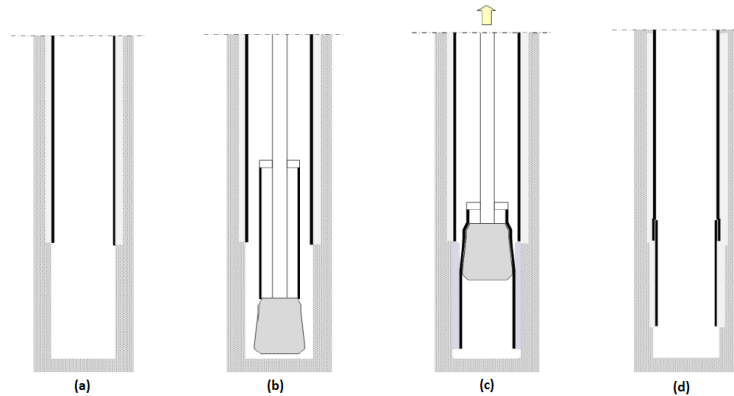


Figure 1.2: Installation of casing using MOD: (a) old casing is cemented in place, (b) new casing with cone and top anchor are run through the previously installed casing, (c) cone is pulled through new casing to expand the diameter and top anchor prevents casing to be pulled upward, and (d) new casing is installed with minimal change in diameter

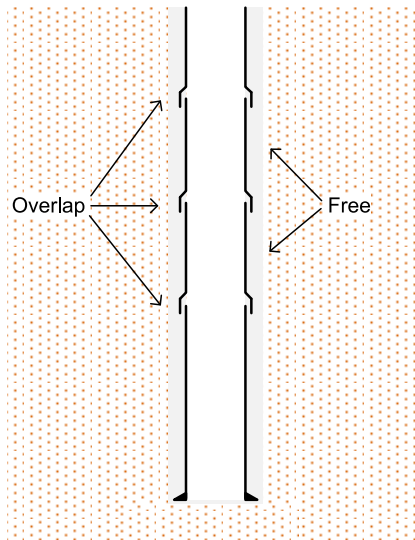


Figure 1.3: Cross-sectional view of an MOD well

After the expansion process, the system of casings has overlap sections at the ends of each casing. In contrast to conventional wells, this well has a single diameter along its length, see figure 1.3 [3], creating a length of the well without (significant) reductions in diameter. This process creates the opportunity for wider diameter inner liners while drilling deeper wells. MOD is developed because wells with a larger inner liner diameter have significant advantages over conventional wells. The most important advantages are:

Economic:

- Required drill bit sizes are reduced. Hence, the size of the rig and consequently the rig rates are reduced;
- Size of wellhead may be reduced;
- Less mud and cement is required;
- Less cutting disposal is created;
- Deeper wells can be drilled, making new reserves more accessible;
- Reservoirs that were shielded by depleted zones are more accessible;
- A large inner liner diameter is maintained; this increases production rate.

Environmental:

- Less rock is cut due to smaller initial bore diameter;
- A smaller surface footprint is left due to a smaller initial bore diameter needed.

During the expansion process the expansion cone is pulled through the casing in order to plastically deform the casing to obtain the permanent larger diameter. The force that is required for this process is referred to as the expansion force. During expansion of the free sections the cone needs to expand the casing in liquid cement. At the overlap sections the cone expands the two casings, the cured cement, and the formation, which requires more expansion force, see figure 1.4[3]. The expansion force causes the drill string to stretch elastically, storing potential energy in the form of strain. At the end of the overlap the contact area between the cone and the casing reduces, friction force decreases, and the cone starts to accelerate. After the overlap area, there is no contact between cone and the casing and the cone pops out. In addition to the resulting force upward, the stretched drill string acts like a spring, contracting to its original length and increasing the acceleration. During the pop-out, the cone movement is viscously damped due to friction between the structure and the fluid. Additionally, a pressure difference over the cone applies a downward force opposite to the displacement of the cone and this has a limiting effect on the cone movement.

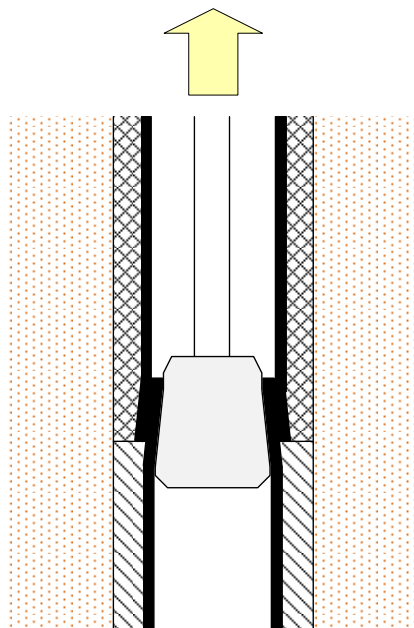


Figure 1.4: Expansion of casing at the overlap

1.2. Cone pop-out

The moment the cone pops out of the casing, it accelerates upwards, leaving a void underneath. Fluids flow through the drill string and through the clearance between the cone and the host pipe, but these flows are not sufficient to fill the void quickly enough. This causes the third flow: the decompression of the bottom hole fluids, see figure 1.5[3]. Due to the limited compressibility of fluids, the volume underneath the cone experiences a severe pressure drop. This pressure change propagates down-hole in the form of a decompression wave. This wave is referred to in this thesis as the swab pressure wave. In addition a compression wave, or surge pressure wave, is propagating from the cone to the surface.

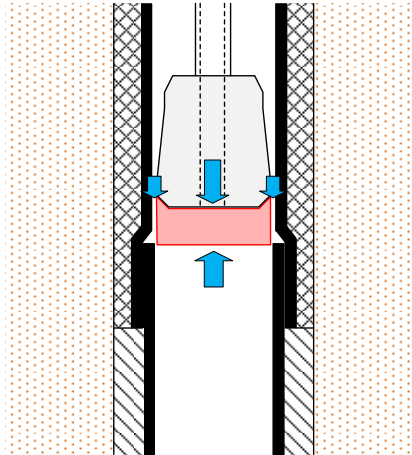


Figure 1.5: Fluid flows during pop-out

The swab pressure in the bottom hole may not exceed the pipe collapse value. The pipe collapse value is calculated according to the API standards [6] and in the case researched in this thesis (10.0" casing, VM50), a collapse value of 150 bar is used. The swab pressure is the difference between the pressure inside and outside the casing, the internal and external pressure respectively. The external pressure consists of the hydrostatic and formation pressure. The internal pressure is influenced by the pressure waves that are created due to the cone pop-out. The swab pressure wave propagates with the speed of sound and is reflected at the bottom; reflection increases the amplitude of the wave. In this research full reflection is used as information on down hole reflection is missing, and therefore a conservative approach is used. The pressure wave will propagate and reflect during this transient phase until a steady-state pressure is obtained. During the transient phase the maximum swab pressure is created. The pressure development in the well is important for the structural integrity of the well. The surge pressure wave propagates to the surface where it dissipates at the end of the fluid column.

This research includes the cone pop-out in wells with depths larger than 5000 meters. In these wells, large hydrostatic pressures are present. Also, the stretch in the drill string is significant in increasing the acceleration during cone pop-out. These conditions can lead to large swab pressures, while cavitation cannot occur. In case of cavitation, water will evaporate and the evaporated water has a much larger volume in the gaseous state. Therefore the fluid flow will be affected significantly.

2

Project overview

The description of previous work is of importance to define the problem statement. This chapter includes the description of two previous graduation projects and the problem definition for this project.

2.1. Problem statement

In 2014 a numerical study [3] has been performed on the cone pop-out phenomenon in mono-diameter wells. In this study, two models are used to calculate swab pressures in mono-diameter wells due to cone pop-out. The models are applied to a case study of the Princess-8 well in the Gulf of Mexico and are based on water hammer theory and theory on pressure surges while running pipe. The governing equations for the fluid domain are solved using the Method of Characteristics (MoC) and the Finite Volume Method (FVM). The research includes analyses on the fluid behaviour, the structural components and the interaction between the two. It is concluded that the fluid-structure-interaction at the cone is dominant for the resultant swab pressure and that the factors that have the largest influence on swab pressure are: expansion force, clearance between cone and host pipe, and bottom hole reflection factor.

Later, in 2015 research was conducted on the validation of the numerical study mentioned earlier. In order to perform the validation of two major factors: the expansion force and the clearance between cone and host pipe, an experiment set-up has been designed by Tillema [4]. Dimensionless flow rates were used to identify critical scaling factors necessary to reduce the size of the experiment. Tillema modified the MoC model for improved calculation on the losses around the cone, and in order to perform calculations for the dynamics in the experiment set-up. Due to constraints the experiment design was not finished and no experiments were performed. In addition, Tillema performed deeper analysis on assumptions from Van Dongen and adjusted the MoC model. The assumption of an instant pop-out was changed in order to take into account the gradually decreasing friction force when the cone exits the casing.

This research includes the design finalising of the experiment, as well as the research of opportunities to mitigate the swab pressure problem. The modified numerical model of Tillema is used in order to specify design requirements and to predict swab pressures during the experiment. The experiment can be executed within the test rig of the Shell Projects & Technology Rijswijk (SPTR) office.

2.2. Experiment

Considering the importance of validation of his models, Van Dongen proposed an experiment set-up. This preliminary design was the basis of Tillema's research and in turn the experiment designed by Tillema is the basis of this research. The final experiment is designed in order to validate the influence of the most important parameters in the numerical model of Van Dongen. Due to research within Shell, the geometry of the cone was found to have a significant influence on the losses around the cone, which influence the swab pressure in turn. Therefore, additions have been made to enable the experiment to verify the effect of a new cone geometry. Also, the fluid properties and behaviour may have an effect on the swab pressure. For that reason the design takes into account that different fluids can be used in the experiment.

2.3. Swab pressure mitigation

The swab pressures are important to take into account in MOD well design. It is interesting to investigate opportunities to reduce the swab pressure in the well, and mitigate the problem. Using current drill string designs in mono-diameter wells, dangerous swab pressures may occur in deep wells, this is described by Van Dongen (2015). In that research flow ports connecting the annulus region with the inner drill string region are suggested, see figure 2.1 [3]. It is important that these flow ports are not simply drilled in the drill string, because that would weaken the strength of the drill string. An assembly should be made that is thicker and as strong as the rest of the drill string, and allows enough flow. This mitigation opportunity is researched further in thesis. The flow ports are numerically implemented in the existing models in order to predict the effect of this mitigation opportunity. Furthermore, an additional flow to fill up the void below the cone is modelled in order to check the requirements and effect on the swab pressure. The goal of researching mitigation opportunities is to estimate the reduction on the swab pressure in the well.

2.4. Approach

The design of the experiment set-up is based on the works of Tillema [4]. In order to finish this design, more detailed aspects had to be researched. Once the detailed design was ready, including production drawings of all parts, the design was checked on Health, Safety Security and Environment (HSSE), and is allowed to be executed in the SPTR test rig. The model of Tillema, finite element analyses and structural strength calculations have been used in order to finish the experiment design, which is described in chapter 3.

The second part of this research consists of developing and numerically testing swab pressure mitigation opportunities. Two opportunities have been researched: the implementation of flow ports above the cone and the influence of additional flow into the system. The flow ports have been added in the existing numerical models using the coupling of the annulus and the inner drill string with an orifice boundary condition. The additional flow has been researched by using an additional flow in the system by fluid stored at the cone. After a difference in pressure that is reached due to normal cone pop-out exceeds a threshold pressure, the fluid is released. The mitigation implementations are described in chapter 4. In chapter 5 the results from the numerical implementation are discussed and in chapter 6 the conclusion and recommendations are given.

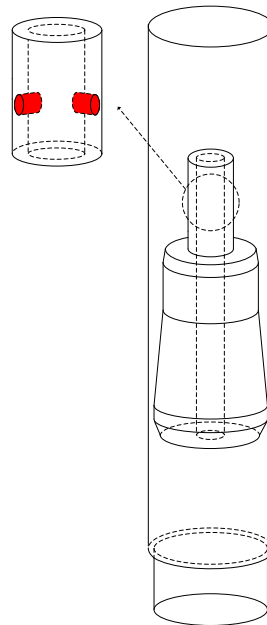


Figure 2.1: The flow ports as suggested by Van Dongen.

3

Experiment set-up

This chapter describes the objective, outline, and the design of the experiment set-up.

3.1. Objective

The experiment has been designed in order to validate the numerical models made by Van Dongen. In the sensitivity analysis of the numerical models, three factors were found that had significant influence on the swab pressure. In order of influence these factors are:

1. Expansion force
2. Reflection factor
3. Clearance

The objective of this experiment set-up is to check the influence of the expansion force and the clearance. The reflection factor is left out of this research because it would effect the size of the experiment significantly. We assume fully reflection in order to have conservative calculations. In addition to the factors stated above the effect of the cone geometry on swab pressure and the effect of viscosity on swab pressure can be checked with the current design. For the cone geometry, a design of the cone with an extended tail is taken into consideration during the experiment and for the effect of viscosity an alternative fluid can be used in the pressure vessel. Therefore the following factors are of interest for the experiment:

- Expansion force
- Clearance
- Effect of cone geometry
- Viscous effects

The influence of these factors on the resulting swab pressure is important in order to validate the models. The validation of these models is important to accurately calculate expected swab pressures, which can be taken into account in well design.

3.2. Outline

In order to explain how the experiment is executed a brief introduction to the experiment execution will be discussed first. Afterwards, the requirements for the experiment and the constraints of the design will be explained. In the subsequent section the components will be described in detail and an elaboration on their selection will be given. In figure 3.1 the final experiment set-up design can be seen in an overview scheme. In this scheme the most important components can be found that will be used to clarify the function of the set-up. A list of the components and their most important functions are given in table 3.1.

In order to describe the experiment execution, the initial conditions and the procedure will be given first. Afterwards the important components will be given along with their most important functions. As an initial condition, the pressure vessel is pressurized to 200 bar. This creates an upward force on the cone due to difference in area below and above the cone, the drill string area. This force presses the moving system (cone and drill string) against the shear pin. This is the only resulting force in the system before the experiment begins.

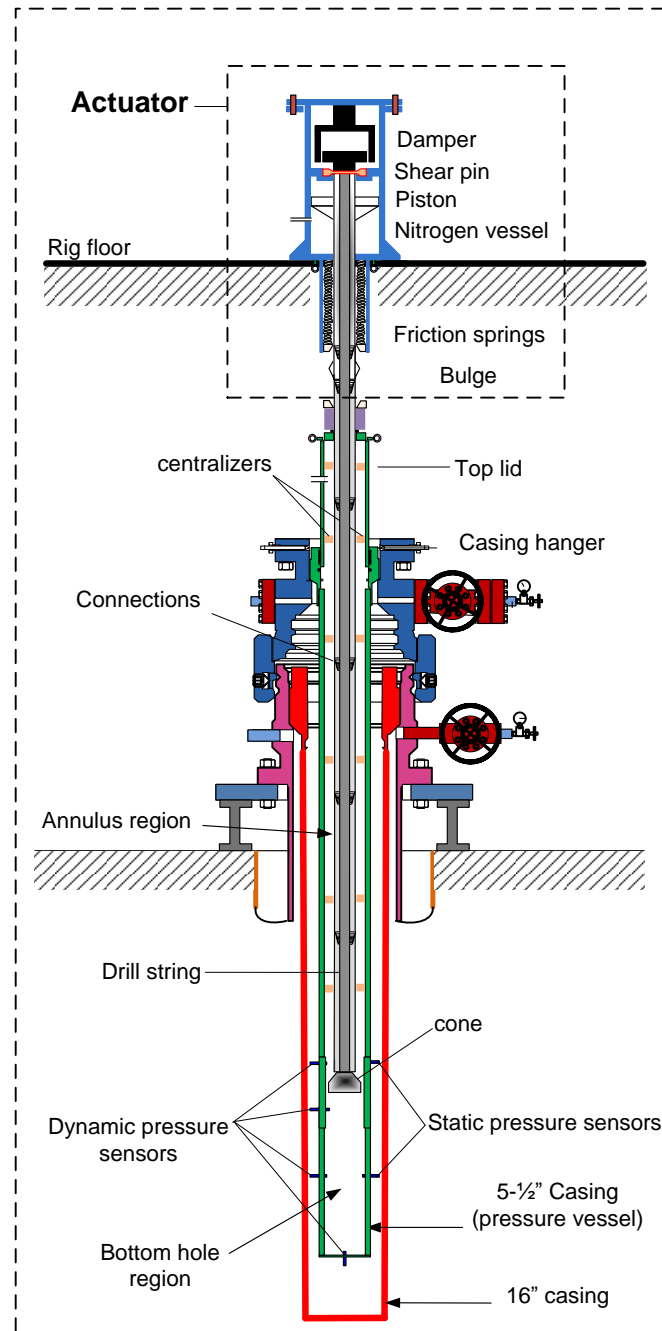


Figure 3.1: The experiment set-up

The procedure of the experiment is as follows:

1. Nitrogen vessel is slowly pressurized until the force on the piston equals the design break force of the shear pin.
2. The shear pin breaks and the piston connected to the drill string accelerate upwards.
3. This acceleration in turn initiates a pressure wave propagating downward inside the drill string.
4. When the pressure wave hits the cone, the cone starts to accelerate and this acceleration is measured from within the cone.
5. The cone acceleration causes a swab pressure wave to propagate downward in the fluid in the bottom hole region and a surge pressure wave to propagate upwards in the fluid in the annulus region.
6. The pressure changes, absolute pressures, and accelerations are measured in order to obtain the useful data necessary for validation.
7. The system is decelerated by the friction springs combined with the damper until force equilibrium is reached between the force generated by the nitrogen pressure on the piston and the force of the friction springs, the damper, and gravity.

In table 3.1 a summary of the components and most important function is given.

Table 3.1: Components of the experiment with their most important functions

Component	Function
Damper	Damp the motion of the top of the drill string to obtain desired kinematics of the cone
Shear pin	Break when the force generated by the nitrogen pressure on the piston that is connected to the drill string exceeds the limit that causes the pin to shear off
Piston	Accelerate the drill string and cone system
Nitrogen vessel	Adiabatic expansion of nitrogen to push piston upwards to mimic pop-out
Friction springs	Apply breaking force and decelerate the moving system and obtain force equilibrium between nitrogen force on piston and force in the springs
Bulge	Get caught in the friction springs to decelerate system
Centralizers	Prevent buckling of the drill string during deceleration
Top lid	Seal off pressure vessel, guide drill string through seal, and handling of the casing by the top drive of the rig
Casing hanger	Hang off the 16" and 5.5" casings and prevent the casings from falling in the hole, it is available at the rig in the SPTR facility
Connections	Connecting drill string parts that are delivered in sections of 3 meters.
Annulus region	Surge pressure wave propagating through annulus that may not disrupt the experiment, therefore annulus region must have a minimum length of 6 meters
Drill string	Connection between actuator and cone, mass influencing dynamics of system, and guide for electrical wire run through
Cone	Necessary for pipe expansion. In the experiment, the geometry determines the fluid flows around the cone, mass influences dynamic behaviour of system, and inside acceleration sensor is placed to
Dynamic pressure sensors	High-frequency measurement of pressure changes
Static pressure sensors	Low-frequency measurement of absolute pressures
5.5" casing	Contain pressure of 200 bar to prevent cavitation in experiments
Bottom hole region	Measurement environment of the swab pressure wave
16" casing	Protection of experiment against open hole

3.2.1. Requirements

The results of this experiment are used to validate the dynamic principles the numerical model is based upon. In order to ensure valuable validation, some critical aspects of the dynamics have to be designed following similar conditions.

The most important aspect is the kinematic behaviour of the cone in the experiment, as this behaviour initiates the pressure wave and the flows to fill the void left below the cone.

Due to the sizing of the test rig in SPTR, the experiment design has been scaled down from a 10.0" expanded casing to a 4.0" expanded casing. In order to maintain the same dynamic behaviour scaling relations have been researched and stated by Tillema and implemented in the previous experiment design[4].

Also, pressure waves propagate through the drill string and are reflected at the ends. The drill string is required to have a sufficient length in order to prevent reflected pressure waves to influence the kinematics of the cone.

Similarly, the annulus region above the cone must be long enough for the pressure wave to propagate in the fluid above the cone. The bottom hole region length is associated with the drill string and annulus lengths because reflections are wanted in the bottom hole region. These relations will be discussed in more detail in section 3.3.1 and 3.3.3.

The actuator has been designed to give the correct acceleration, constant velocity and quick deceleration of the system. Due to spatial limitations of the test rig in the SPTR facility and to allow for easier handling, the actuator is designed to be compact and be able to be mounted to the rig floor. It is limited in height in order for personnel to safely access the shear pins when these need to be changed.

3.2.2. Constraints

The most important constraint is the dimensional limitation associated with the stroke that the rig can make in order to install the components of this experiment. The total stroke the rig can make is 14.7m from the rig floor upward. Since the total set-up is longer than this given length, the installation has to be done in parts that can be connected above the rig floor, or underneath the rig floor.

The drill string length is dependent on the selected material and the measurement time. The time it takes pressure waves to travel up and down the drill string must be longer than the measurement time. The Young's modulus and density determine the speed of sound (and thereby the speed of the pressure waves) through the material. If the speed of sound is high, a long drill string is needed. The longer drill string will have more mass and this will influence the forces and stresses in the system.

In this experiment, the length of the drill string does not allow the rig to pull the entire drill string in one stroke out of the casing. For experiments with different cones this means that the drill string has to be broken and made up again. To be able to perform these proceedings, space is necessary where personnel can safely access the drill string.

The 16" casing can be safely mounted to the standard 16" casing hanger that is available at the SPTR facility. A shoulder is developed in order to allow the 5.5" casing to be hung off the smaller casing hanger.

The actuator is mounted to the rig floor, and the system of the cone and drill string is able to move freely in vertical direction. During the deceleration phase, the moving system is decelerated by the actuator. The actuator is connected to the rig floor, therefore the rig floor also has to be able to withstand the loads in the experiment. The capacity of the rig floor has to be checked for the maximum load cases before the experiment is executed. If necessary, the connection to the rig floor needs to be fortified.

3.2.3. Experiment execution

This section gives a description how the actuator initiates and stops the experiment. It is necessary to introduce this procedure before the components will be discussed. Four steps will be described and later in this chapter the details per component will be given, see figure 3.2. The dimensioning of the set-up and the

actuator can be found in Appendix A.

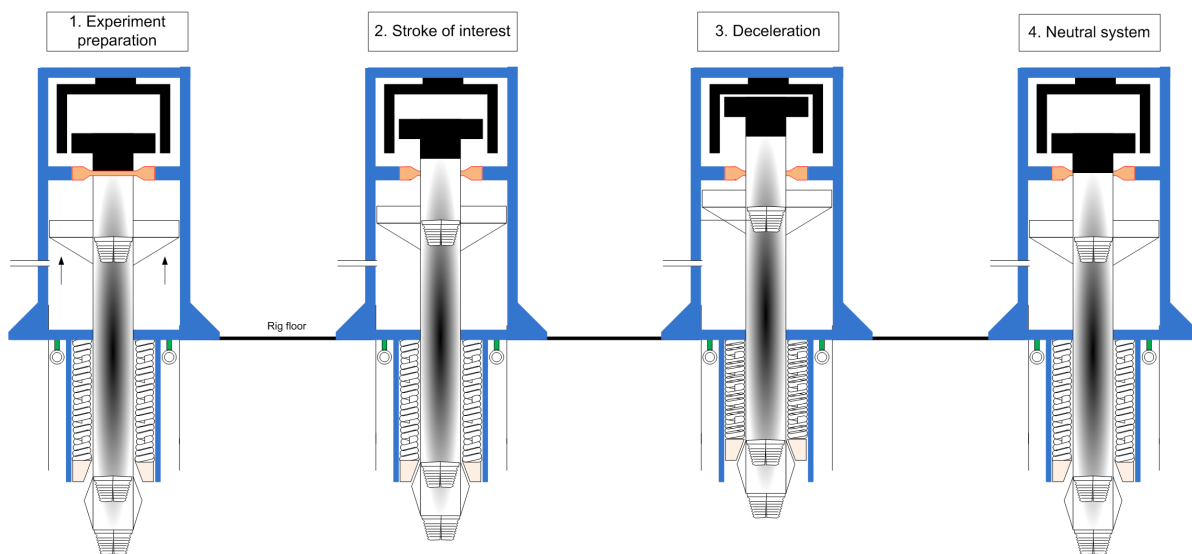


Figure 3.2: Schematic drawing of the actuation and deceleration mechanism.

Experiment preparation

The experiment assembly and handling plans can be found in Appendix B. The experiment can be controlled by the pressure in the pressure vessel filled with water and the pressure in the nitrogen vessel. The fluid pressure is more difficult to accurately control than the nitrogen pressure due to the difference between the bulk modulus of water and the expansion factor of nitrogen (gas expands much more than a fluid and therefore is easier to exactly pressurize). At the start of preparation there is no added pressure in either vessel in order to safely place the shear pin. When the shear pin is placed, first nitrogen pressure is used to lift the drill string and press it against the shear pin that will press in turn against the damper. When correctly placed, the pressure vessel containing water is pressurized to 200 bar. The load cases in the experiment are displayed in table 3.2.

Table 3.2: Load cases of the experiment

Load case	Unit	Low value	Middle value	High value
Maximum shear pin load	[mT]	27.2	32	36.8
Equivalent expansion force	[kN]	267	314	361
Nitrogen pressure	[bar]	79.9	95.7	111
Cone OD experiment	[mm]	99.568	100.584	101.6
Cone OD experiment	["]	3.92	3.96	4.00
Equivalent real cone OD	["]	9.8	9.9	10.0
Scaling factor of cone OD	[-]	0.4	0.4	0.4

Stroke of interest

The first 100mm the cone will displace is the stroke of interest. During this stroke the measurements have to be made in the pressure sensors and the acceleration sensors. After the stroke of interest, the bulge will hit the friction springs and this will create pressure waves that will influence the motion of the cone. At the end of the stroke of interest a pressure remains inside the nitrogen vessel pushing the piston upwards, this needs to be compensated by the set of friction springs during the deceleration of the system.

Deceleration

The cone experiences a constant velocity due to the damper used, but when the bulge hits the friction spring assembly the deceleration is initiated. At this moment, the piston experience a reduced nitrogen pressure due to volume expansion, but this force needs to be taken up by the spring. By using friction springs energy is taken out of the system due to friction.

Original system

When the experiment is complete and the system is in rest, forces remain on the piston and the friction spring. In order to safely bring the system to a neutral position, first the pressure is decreased in the pressure vessel containing water. Afterwards the nitrogen pressure is reduced slowly, making sure the drill string does not fall down, but gently lowered. In this case, the bulge can be placed on the top lid of the pressure vessel, supporting the drill string and piston. Once the bulge is placed, the nitrogen pressure can be decreased further and experiment settings can be changed. The proceedings necessary to change between cones or shear pins can be found in Appendix B. Also the design of experiment, the order and settings of all runs, is displayed in Appendix B.

3.2.4. Force calculations

In this section, the forces are determined for each stage of the experiment. All calculations have been performed using the highest load case: 36.8mT. The relevant parameters are displayed in tables 3.3 and 3.4. Figure 3.3 is a schematic overview of the main tensile- and compressive loads during the three stages of the experiment.

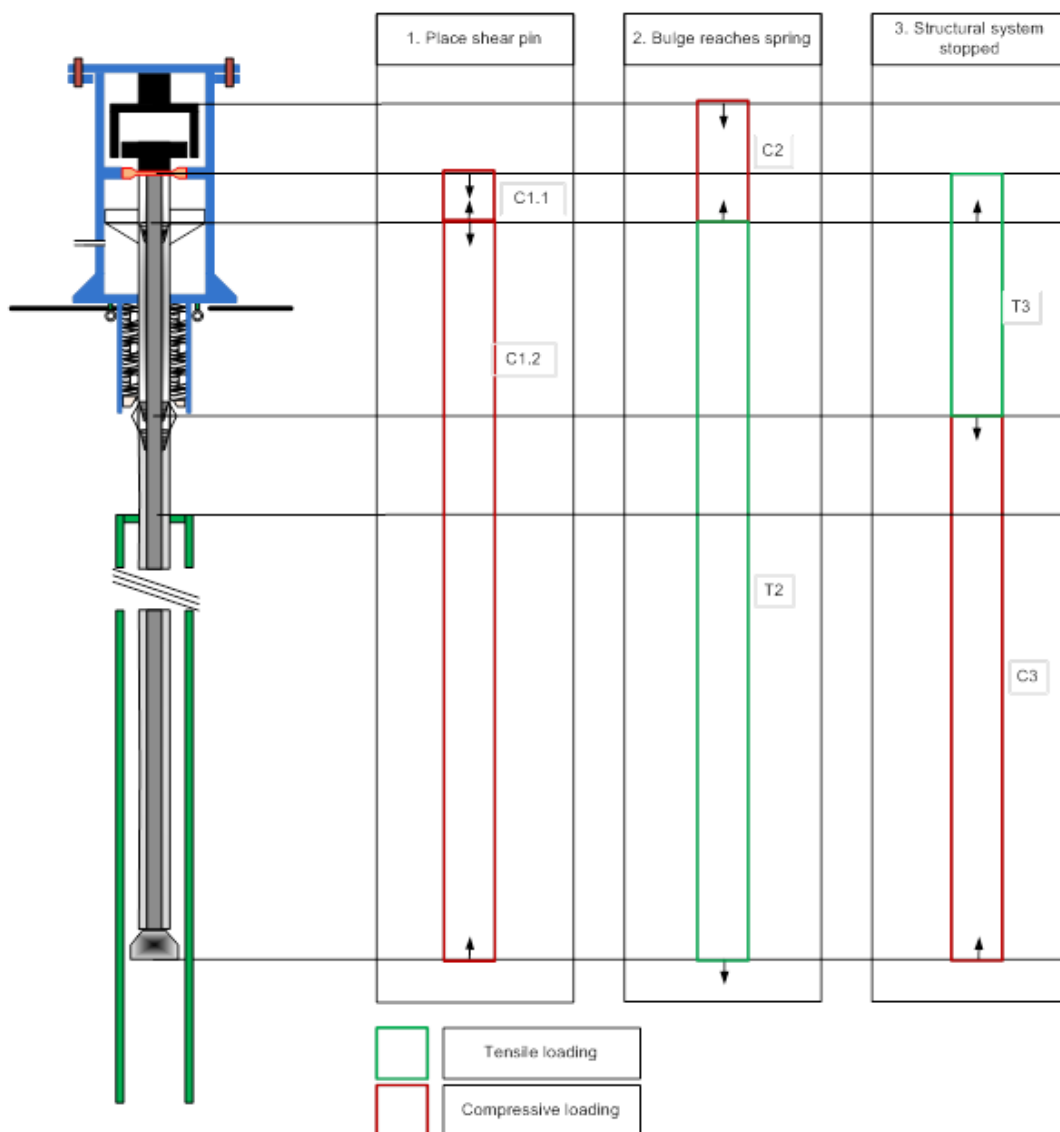


Figure 3.3: Free body diagram of the compressive and tensile loads during the experiment

Table 3.3: Relevant parameters in actuator design

Parameter	Value	Unit
Shear pin break load	36.8	[mT]
Expansion force	361	[kN]
Piston area	2.98	[m ²]
Nitrogen pressure at shear pin failure	111	[bar]
Initial height nitrogen chamber	0.8	[m]
Heat capacity ratio nitrogen	1.4	[-]

Table 3.4: Relevant parameters in drill string design

Parameter	Value	Unit
E modulus	197	[GPa]
Density 17-4 PH	7850	[kg/m ³]
Drill string ID	0.01	[m]
Drill string OD	0.045	[m]
Surface area drill string	1.51e-3	[m ²]
Second moment of area	2.01e-7	[m ⁴]

Pressures

The pressures in the nitrogen vessel for the different stages are given in table 3.5. The nitrogen pressure can be calculated easily if isentropic (reversible adiabatic) behaviour is assumed [7]:

$$P_{nitrogen,t+\Delta t} = P_{nitrogen,t=0} \left(\frac{V_{nitrogen,t+\Delta t}}{V_{nitrogen,t=0}} \right)^{-\gamma} \quad (3.1)$$

With $\gamma = C_p/C_v = 1.4$ for nitrogen. C_p is the specific heat at constant pressure, C_v is the specific heat at constant volume, and γ is the specific heat ratio [8].

Table 3.5: Gas pressures and pressure forces for each stage of the experiment

	Unit	Stage 1	Stage 2	Stage 3
Height nitrogen chamber	[m]	0.8	0.9	1.2
Pressure nitrogen chamber	[bar]	111	94.5	63.2
Volume nitrogen chamber	[m ³]	1.92e-2	2.16e-2	2.88e-2
Nitrogen pressure force on piston	[kN]	332	282	188

Energy balance

During the deceleration, the friction springs dissipate energy to stop the structural system. The characteristics of the friction springs are chosen to achieve a balance in energy between the potential energy of the pressurized nitrogen, the kinetic energy of the system, the damper and the friction springs.

$$E_{P,nitrogen} + E_{Kin} - E_{damper} - E_{frictionsprings} = 0 \quad (3.2)$$

$$E_{frictionsprings} = E_{P,nitrogen} + E_{Kin} - E_{damper} \quad (3.3)$$

The energy that is associated with the pressure of the nitrogen is:

$$E_{P,nitrogen} = F_{P,nitrogen}^{average} * s_{deceleration} \quad (3.4)$$

Where $F_{P,nitrogen}^{average}$ is the average value of the nitrogen pressure force during deceleration and $s_{deceleration}$ is the deceleration stroke, calculated with the help of FEA to be 0.23m, see Appendix C

The kinetic energy is calculated by:

$$E_{kin} = \frac{1}{2} M_{system} v_{max}^2 \quad (3.5)$$

Where M_{system} is the mass of the structural system and v_{max} is the velocity just before deceleration.

Table 3.6: Values for calculation of the potential energy of the pressurized nitrogen

Parameter	Value	Unit
Average force during deceleration	272	[kN]
Deceleration length	0.23	[m]
$E_{P,nitrogen}$	62.6	[kJ]

Table 3.7: Values for calculation of the kinetic energy in the system

Parameter	Value	Unit
M_{system}	365	[kg]
v_{max}	5.3	[m/s]
E_{kin}	5.13	[kJ]

The energy absorbed by the damper is calculated as follows:

$$E_{damper} = F_{damper} * S_{deceleration} \quad (3.6)$$

$$F_{damper} = c_{damper} v_{avg}^2 \quad (3.7)$$

Where v_{avg} is the average velocity during deceleration. Assuming a linear deceleration, this is 2/3 of the maximum velocity. c_{damper} is the damping constant belonging to the damper. The damper used is a damper with a squared damping constant, therefore the damping force is related to the velocity squared.

Table 3.8: Values for calculation of the energy taken up by the damper

Parameter	Value	Unit
Average velocity during deceleration	3.53	[m/s]
c_{damper}	11050	[Ns ² /m ²]
E_{damper}	31.7	[kJ]

With these values, the energy that the friction springs need to absorb is $62.6 + 5.13 - 31.7 = 36.03$ kJ. With this information, the force that the friction springs have to be able to take up can be calculated:

$$F_{frictionsprings} = \frac{2 * E_{frictionsprings}}{S_{deceleration}} = 313kN \quad (3.8)$$

Forces in drill string

In figure 3.3 the main tensile- and compressive loads have been displayed. The following equations show how the compressive forces are calculated. The forces are displayed in table 3.9.

$$C1.1 = F_{P,nitrogen} + F_{water} - M_{system} * g \quad (3.9)$$

$$C1.2 = F_{water} - M_{system} * g \quad (3.10)$$

$$C2 <= F_{P,nitrogen} + F_{water} - M_{system} * g \quad (3.11)$$

$$C3 = M_{system} * d \quad (3.12)$$

Where $F_{P,nitrogen}$, is the nitrogen pressure force working on the piston, given in table 3.5, $F_{water} - M_{system} * g$ is the resultant pressure force of the water pressure on the effective surface on the cone, minus the weight of the system. This is the surface of the drill string area (without deduction of the inner drill string area). This is the area that does not experience the pressure from the upside of the cone and the bottom of the cone, creating a resulting pressure force pointing upwards. And d is the rate of deceleration ($d = \frac{v_{max}^2}{2 * S_{deceleration}} = 61m/s^2$). It is difficult to calculate F_{water} exactly during stage 2 and 3 due to the pressures under the cone, because of the interaction of the swab, surge and hydrostatic pressures. In order to remain conservative, the initial water pressure is used to determine the compressive forces. The tensile forces are calculated with the following equations:

$$T2 = \frac{v_{max} A_{ds} E_{ds}}{c_{ds}} + M_{system} * g \quad (3.13)$$

$$T3 = F_{P,nitrogen} - F_{frictionsprings} - M_{system} * g \quad (3.14)$$

Table 3.9: Overview of tensile- and compressive forces

Load case	Force [kN]
C1.1	361
C1.2	28.5
C2	361
C3	22.3
T2	319
T3	72.3

The compressive loads C1 and C2 determine the strength required in the drill string, and determine the forces in the buckling calculations to define the maximum unsupported length. The load T2 determines the maximum tensile force the connections in the drill string need to take up.

3.3. Design

Performing a real pipe expansion with measurement equipment down-hole would cause difficulties in repeating experiments under exactly the same conditions. The pipes to be expanded often show irregularities (in ovality, eccentricity, and wall thickness) and therefore it is very difficult to repeat experiments that include pipe expansion. After each expansion process a new pipe would have to be installed at the same depth, but it is very difficult to maintain exactly the same conditions. This experiment is designed to be performed on a smaller scale in the test rig in the SPTR facility. The design enables easy access to the actuator and is made to minimize the proceedings to change experiment settings. Also, no actuation equipment is present in the bottom hole that may disrupt the pressure wave initiated by the cone acceleration [4].

The following sections will describe the most important components in the design:

- The drill string connecting the actuator to the cone. The electrical wire connected to the accelerometer in the cone is run through the drill string.
- The cone that has different shapes and sizes in order to check the effect of clearance between cone and host pipe and the effect of a different geometry of the tail of the cone.
- The pressure vessel in which the swab pressure wave will propagate.
- The actuator that initiates the acceleration of the cone.

In turn, these components are made up of smaller components that will be discussed in each section.

3.3.1. Drill string

In the experiment the drill string connects the actuation mechanism that is placed above the rig floor to the cone in the water vessel, see figure 3.1. Additionally, an electrical wire is connected to the accelerometer and is run through the drill string. The drill string needs to be strong enough to prevent deformation and long enough to prevent an acoustic wave from disturbing the experiment down hole. During the actuation procedure of the experiment a pressure wave propagating through the drill string initiates cone acceleration and reflects on the ends of the drill string. To prevent this wave disturbing the experiment, its length and speed of sound have to be in balance with the length of and speed of sound in the bottom hole. For the experiment one reflection down hole and one reflection at the cone will be studied, requiring three lengths of the bottom hole for the pressure wave propagation. The pressure wave in the drill string, once reflected off the cone and propagating upward, may not reach the cone again before this is finished; this requires a minimum of two lengths of drill string.

$$3 \frac{L_{bottomhole}}{c_{bottomhole}} < 2 \frac{L_{ds}}{c_{ds}} \quad (3.15)$$

Dimensions

The drill string has been scaled in radial direction together with the other components in the setup, and in longitudinal direction according to the formula above. The outer diameter (OD) of the drill string is 45mm, scaled down from a real-size 4.5inch drill string. Considering there is no flow through the drill string in the experiment, this should not cause problems for the validation. The inner diameter (ID) is not scaled, but is chosen as a minimum to allow the cabling for sensors in the cone to be traced through and to maximize the strength of the drill string.

Material

Two properties of the material of the drill string are important in this experiment: the yield strength and the speed of sound through the material. The yield strength is important because the drill string is subjected to very high tensile and compressive loads during the experiment. The standard drill string material (steel) will not be strong enough and locally the material will deform plastically. For this reason a stronger material needs to be selected. The speed of sound through the material is important because during the acceleration of the system sound waves will propagate through the material and these may not disrupt the experiment results that are measured underneath the cone. The length of the drill string also influences the total mass of the moving system and thereby the forces in the connections. During an iterative process that investigated the trade-off between speed of sound in the material and strength, a final material 17-4 PH stainless steel has been selected, with an Ultimate Tensile Strength (UTS) of up to 1379 MPa and a 0.2% yield strength of up to 1345 MPa[9].

Connections

The connections in the drill string are the weak spots because the effective area taking up compressive and tensile forces is reduced. Different connections have been researched in order to select the most effective. Finite Element Analyses (FEA) have been performed using the load cases in the experiment in order to determine maximum tensile and compressive forces the drill string undergoes. The design of the most effective connection is a standard NC13 connection with adjusted shoulders to take up the high compressive loads. The FEA results in figure 3.4 show local maxima of 1375.7 MPa, but the next highest values consist of stresses of 730 MPa. Due to these high stresses found, which just exceed the yield strength of the material, it is advised to test a sample connection.

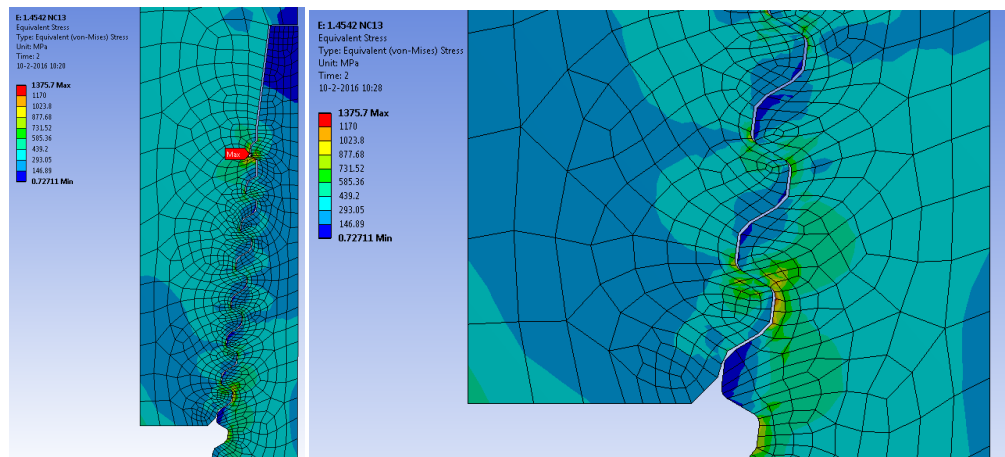


Figure 3.4: FEA results from a 36.8 metric tonnes tensile load, performed by Callidus Group.

Centralizers

Centralizers are connected to drill string sections in order to prevent buckling during the deceleration process. Buckling is most likely to occur right under the bulge where the deceleration is initiated. This is the position where the system experiences the most mass decelerated, namely the mass of the drill string length from bulge to cone plus the mass of the cone. The buckling length for an unsupported rod is [10]:

$$L_{buckle} = \sqrt{\frac{\pi^2 EI}{F_{buckle}}} \quad (3.16)$$

Where

$$I = \frac{\pi(OD^4 - ID^4)}{64} \quad (3.17)$$

With $E = 197\text{GPa}$ [9], $OD = 45\text{mm}$ and $ID = 10\text{mm}$.

In order to make sure that the drill string will not buckle during the deceleration, it is important that the maximum unsupported length is shorter than the values in table 3.10 for the defined sections. For safety, at every drill string length, approximately 3m, a centralizer is placed in the pressure vessel. The centralizers are made from composite and can be glued together to become light and easily connected to the drill string, see figure 3.5. In the highest load case, a force of 361kN is working on the part between the piston and the damper, using the same formula a buckling length of 1.04m is found. The length of this part of the drill string is 0.5m and is therefore safe from buckling.

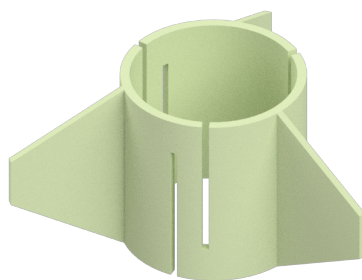


Figure 3.5: Design of the centralizers

Table 3.10: Maximum unsupported length in experiment per load case

Load case	C1.1	C1.2	C2	C3
Buckling force [kN]	361	28.5	361	22.3
Buckling length [m]	1.04	3.70	1.04	4.18

3.3.2. Cone

The fluid flows around and through the cone determine the minor pressure losses that are significant for the generated swab pressure, making the cone geometry very important. The cones used in this experiment are extended on the upstream side in order to add mass. The inertia of the cone is very important due to the oscillating behaviour that needs to be reproduced. The effect on the fluid flows by the different geometry is taken into account in the numerical models that are used to check the working of the experiment. The effect of this extension does not significantly change the fluid flow behaviour around the cone.

Original cone design

The original cone design has the same angles and lengths as the cone used for expansion purposes in practice at this day. The angles have been optimized for the expansion process, but not for the fluid flows that affect the minor losses during pop-out. During previous research performed by Shell, a new design of the cone is suggested in order to get preferred fluid flow behaviour. The cones used in this experiment have the same outer geometry as the real cones.

Cone with extended tail

The geometry of the tail of the cone influences the recirculation area downstream and does not change the expansion process. In order to reduce the recirculation area of the cone, a new geometry is suggested. Computational Fluid Dynamics (CFD) calculations promise good behaviour of this cone with alternative geometry and a 30% reduction in minor losses is estimated by Shell. If this percentage is realized, in total approximately 9-10% of the swab pressure may be reduced with this alteration to the cone geometry. This additional cone design is added to the experiment to validate these calculations.

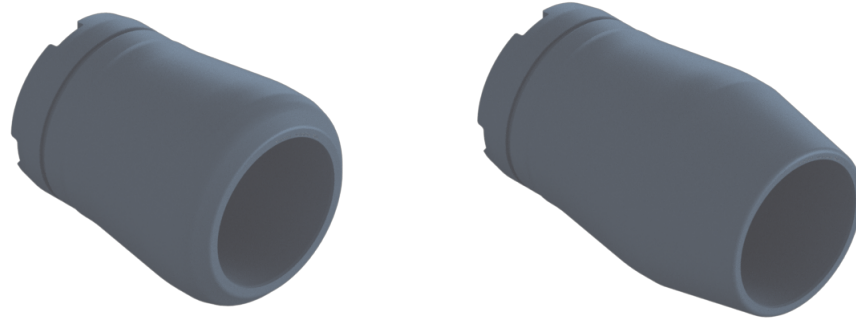


Figure 3.6: The original cone (left) and the cone with extended tail (right)

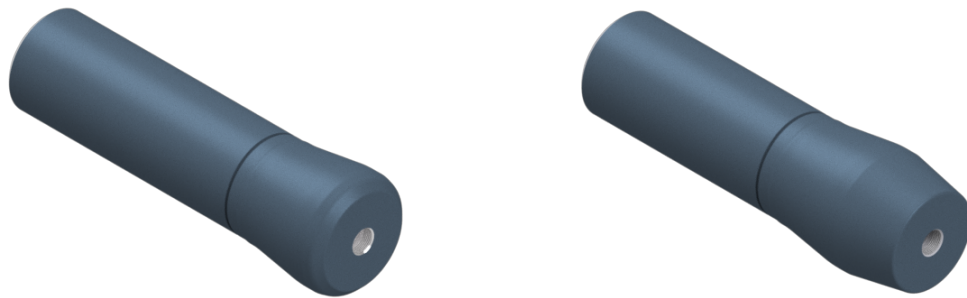


Figure 3.7: The normal cone used in the experiment (left) and with extended tail (right)

3.3.3. Pressure vessel

In figure 3.1 the pressure vessel is the green casing underneath the rig floor. In order to prevent cavitation underneath the cone during acceleration, the pressure vessel in the experiment is filled with water and pressurized to 200 bar. Other important features of the pressure vessel are the length of the bottom hole, length of the annulus, and the inner radius of the casing where the cone is accelerated. This location is of importance because changes in the diameter at this position cause the clearance to deviate from the required clearance. As the effect of the clearance is one of the parameters to be validated by this experiment, it is important that precision is used in machining this part. This section has to be machined to 0.02mm accuracy to have a maximum deviation in results of 2.14% [4].

Bottom hole

The bottom hole section around the cone is machined to a specific diameter (0.02mm accuracy) in order to ensure the effect of the clearance between the cone and this section is according to the real situation. The clearance determines the flow rates, which in turn determine the frictional losses over the cone. The rest of the bottom hole is also machined accurately in order to avoid any minor losses due to the geometry of the inside of the vessel.

Annulus

The surge pressure wave above the cone may not have an influence on the measurements in the bottom hole, so the time it takes for the surge pressure wave to propagate to the top of the annulus and back should be longer than the 3 lengths, or two reflections, measured in the bottom hole.

$$3 \frac{L_{bottomhole}}{c_{bottomhole}} < 2 \frac{L_{annulus}}{c_{annulus}} \quad (3.18)$$

The suggested dimensions and tolerances are given in table 3.11.

Table 3.11: Dimensioning of the pressure vessel

Section	OD ["]	OD [m]	Wall thickness [mm]	Tolerance [mm]	Length [m]
Top lid	5.5	0.1397	29.4	0.1	2.1
Annulus region	5.5	0.1397	13.462	0.1	25.0
At the cone	5.5	0.1397	18.05	0.02	1.5
Bottom hole region	5.5	0.1397	18.05	0.2	3.65

3.3.4. Actuator

As discussed in section 3.2.3, the system is accelerated using a gas spring pushing a piston upwards. The piston is connected to the drill string that presses against a shear pin. The pressure is built up until a specific threshold force is reached that forces the drill string through the shear pin, accelerates the system for 100mm until the bulge reaches the spring. The spring decelerates the system and a force equilibrium is reached between the remaining force from the gas spring and pressure in the water vessel upwards and the force from the spring on the bulge downwards. The energy is taken out of the system by removing the water pressure and gas pressure respectively until the spring is back in its original position.

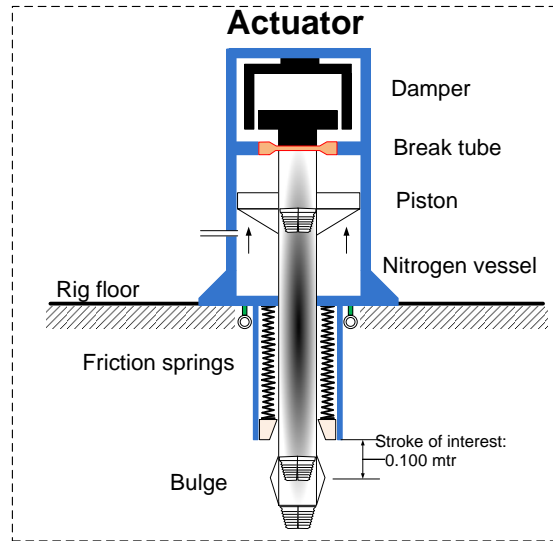


Figure 3.8: Schematic drawing of the actuator.

Nitrogen vessel

The combination of the piston and the nitrogen pressure acting on the piston is the actuation mechanism of this experiment, as designed by Tillema [4]. The nitrogen vessel is designed to deliver the correct initial force on the piston during push-out. The equations in this section have been used to calculate the pressures stated in section 3.2.3. The governing equations for the accelerating system are:

$$M_{piston} \frac{\delta^2 u(z_{piston}, t)}{\delta t^2} = E_{ds} A_{ds} \frac{\delta u(z_{piston}, t)}{\delta z} - c_{damper} v_{piston}^2 + F_{P,nitrogen} + F_{water} \quad (3.19)$$

To decelerate the system a spring is placed and the system is decelerated by a bulge that shoots inside a cylindrical spring, the governing equation is:

$$M_{piston} \frac{\delta^2 u(z_{piston}, t)}{\delta t^2} = E_{ds} A_{ds} \frac{\delta u(z_{piston}, t)}{\delta z} - c_{damper} v_{piston}^2 - k_{spring} u(z_{piston}, t) + F_{P,nitrogen} \quad (3.20)$$

Note that the damping factor is coupled to the piston velocity squared (squared damping constant), this is under the assumption that the piston and end of the drill string velocities are the same: the upper part of the drill string is considered rigid. Also note that the force executed by the water on the drill string area is not taken into account in the deceleration stage. There will be a positive pressure working on the drill string area, but as discussed earlier it is difficult to determine the pressure right under the cone, therefore for conservative reasons this force is not taken into account.

The pressure force by the gas on the piston is:

$$F_{P,nitrogen} = A_{piston}P_{nitrogen} \quad (3.21)$$

The resultant upwards force, with pressurized water vessel and no pressure in the nitrogen vessel (these are the initial conditions of the experiment), due to the pressure in the the water vessel is:

$$F_{upwards} = A_{ds}P_{water} - (V_{cone} + V_{ds}) * \rho_{ds} * g - (V_{cone} + V_{ds} + V_{ds,i}) * \rho_w * g - M_{piston} * g \quad (3.22)$$

The first term in the equation is the pressure force over the drill string area. The drill string area only experiences the pressure from the water at the bottom, therefore the resulting force is taken into account. The second and third terms together form the resulting buoyancy force exerted by the water, and the third term is the weight of the piston. The velocity profile of the cone is aimed to be as constant as possible until the bulge hits the springs. The velocity profile for the design is estimated using the Finite Element Analysis model 4RealSim has made, see Appendix C.

Piston

Two piston designs have been made in order to comply with the strength requirements. One is designed for the production with a titanium 3D printer, the other to be machined using the same steel as the drill string, see figure 3.9. The advantage of the titanium piston was that it is lightweight and can be produced in the titanium 3D printer in the Amsterdam Shell location. The machinable design did not show significant change in performance in the numerical models.



Figure 3.9: The old titanium-printed piston design (left) and the steel machinable piston (right).

Shear pins

Shear pins have been applied in other designs within MOD tests in the SPTR facilities and the design for this experiment is based on those tests that have been conducted successfully. However, the shear pins produced were tested in the Callidus Group facility in Joure and in the SPTR facility, but they showed very different results.



Figure 3.10: The current shear pin design.

The shear pin design in figure 3.10 has been tested in a press in order to verify the breaking force. If the design is able to be broken within a close range of the aimed force, this design can be used for the experiment. However, the tests performed in the Callidus Group test facility and that in SPTR showed considerable different results, see figure 3.11.

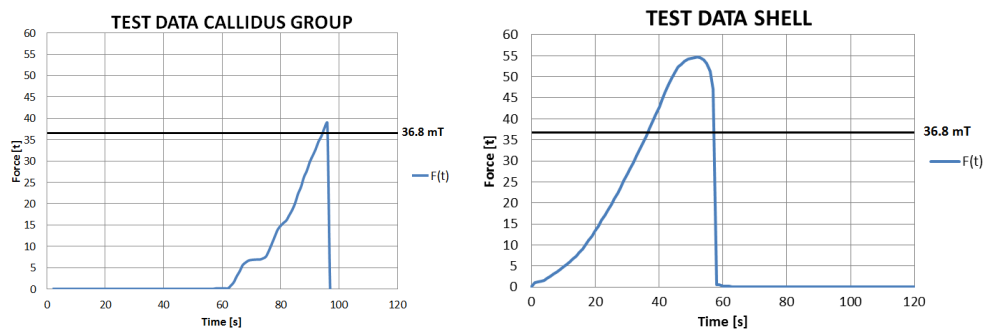


Figure 3.11: The shear pin verification performed by Callidus (left) and Shell (right).

Because of the difference in results in the shear pin design it is recommended to design a new concept before the experiment will be conducted. The requirements for the shear pins are:

- No ductile behaviour, an instant brittle break is desired;
- The forces to break the shear pins for the all load cases are 267, 314, and 361 kN.

Damper

A commercially available damper with a squared damping constant of $11050 \text{ N}(s/m)^2$ is found for the experiment [4]. This damping constant is necessary to create similar kinetic behaviour of the cone. The damper is chosen to keep a constant velocity profile of the cone for the 100mm of interest. The full stroke of the drill string is 400mm and so is the maximum damper stroke. For this length minus the 100mm stroke of interest, a set of friction springs is selected to assist in decelerating the system.

Friction springs

Friction springs are chosen for the deceleration of the system to absorb energy by friction. The friction springs chosen are the Ringfeder 16600 [11]. The force the springs are required to endure is at least 313 kN as calculated earlier in this chapter. These springs can take up a maximum load of 350 kN. The maximum stroke of the spring is 300mm, after this length the maximum stroke of the experiment is reached and the damper will reach its maximum stroke. A spring coefficient of maximum 0.9kN/mm is wanted in order to minimize the compressive force in the drill string during deceleration. The total work to be performed by the friction springs during this stroke is a minimum of 36 kJ. A set of 106 rings is selected that has characteristics displayed in table 3.12.

Table 3.12: Characteristics of the 16600 Ringfeder friction spring

	value	unit
Spring number	16600	[-]
Height of ring	20	[mm]
Stroke per ring	3.7	[mm]
Mass per ring	0.869	[kg]
Work per ring	0.648	[kJ]
k_{ring}	94.6	[kN/mm]
k_{spring}	0.8924	[kN/mm]
Maximum force	350	[kN]
Number of rings	106	[-]
Maximum work	68.7	[kJ]
Length uncompressed	2120	[mm]
Mass spring	92.1	[kg]
Added mass spring	37.7	[kg]

It can be seen in the table that the spring coefficient is below the 0.9kN/mm that is required and the total work the spring can perform is sufficient. The length of the spring is short enough for installation underneath the rig floor. The added mass will not influence the experiment since the spring will be used after the stroke of interest. Following the FEA analysis performed by 4RealSim, see Appendix C, with these settings the displacement of the structural system is less than 400mm and of the spring less than 300mm. For that reason, the spring (300mm stroke) and damper (400mm stroke) can be used.

3.3.5. Sensors

The measurement environment in this experiment consists of multiple pressure sensors in the bottom hole and annulus, plus a tri-axial acceleration sensor in the cone, and a mono-axial acceleration sensor near the damper.

Pressure sensors

There are two kinds of pressure sensors near the cone: static and dynamic pressure sensors. The static pressure sensors measure at low frequencies and are used to validate the absolute pressures around the cone in each experiment. The dynamic pressure sensors measure at high frequencies (25-50kHz) and are used to record the pressure changes due to the swab pressure wave in the bottom hole and the surge pressure wave in the annulus. In the bottom hole, several sensors are placed in order to measure the amplitude of the pressure wave. By using two dynamic pressure sensors in the wall of the casing bottom hole, information on the wave front can be obtained. The pressure sensor in the bottom of the casing records a third measurement in the middle of the water column and measures the reflection of the pressure wave.

Acceleration sensors

In order to validate the kinematics of the actuation mechanism and most importantly of the cone, two acceleration sensors are placed, one next to the damper and the other inside the cone. The acceleration in the cone is measured by a sensor connected to the electrical wiring that is run through the drill string. This is the reason for the hollow drill string used in this experiment (if newer technologies will allow a guaranteed data collection for this experiment, it is advised to use a solid rod for a drill string; this will allow using a material with a lower Young's modulus and higher density, in turn a lower speed of sound through the drill string, allowing a shorter drill string and significantly reducing the number of proceedings to change the cones).

4

Swab pressure mitigation

There are several factors that influence the magnitude of the swab pressure that is created due to cone pop-out. As stated in the previous chapter the expansion force, reflection factor, and the clearance were found in a sensitivity analysis [3] as the most important three factors. The expansion force needed for pipe expansion may not be reduced, the liner diameter change desired is given and the reflection factor is out of the scope of this research. Other factors influencing the swab pressure are for that reason analyzed. In recent research, valves connecting the annulus and the flow through the drill string were suggested for a possible way to reduce the swab pressure in the bottom hole. A swab pressure wave propagates from the cone downwards, but simultaneously a surge pressure wave is propagating upwards in the annulus. The swab pressure also propagates through the drill string upwards, because this is directly connected to the bottom hole area. The pressure difference between the inside and the outside of the drill string is used to create a flow, when flow ports are placed. This flow increases the nozzle flow through the drill string and reduces the bottom hole expansion. In figure 4.1 [3][4] the flow rates for the situation without flow ports are shown, for the case study performed. The case that is used as a base case in this research is the second liner of the P8 well in the Princess Field in the Gulf of Mexico. The most important difference between the two models is that in the model with a gradual decrease in expansion force, the development of the flows is also more gradual, and the contribution of the flow through the clearance is initiated when the gradual decrease is done. This is the moment the cone pops out of the expandable casing.

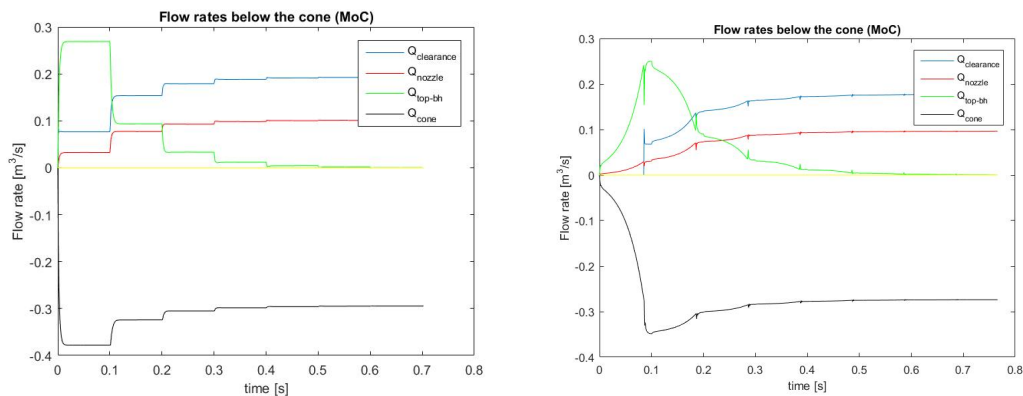


Figure 4.1: Flowrates below the cone in the normal model (left) and the model with gradual decrease of expansion force (right)

Figure 4.1 shows that in the first moment after pop-out, the bottom hole expansion (flow rate out of the top of the bottom hole, green line) has a large contribution in filling the void that is left underneath the cone. The expansion of the fluid column is the cause of the decompression and this determines the magnitude of the swab pressure. When focusing on the flow rates, possibilities to reduce the contribution of the bottom hole expansion are:

- Increasing the flow through the nozzle
- Increasing the flow through the clearance
- Introducing an additional flow in the system

Increasing the flow through the nozzle may be possible by the flow ports. The shape of the cone cannot be changed because it affects the expansion process. In addition, the size of the clearance cannot be changed because it is related to the well design and the expansion force. For those reasons, the flow through the clearance cannot be changed. Third, a flow may be added into the system in order to decrease the bottom hole expansion.

The flow port principle increases the flow through the drill string to fill up the void that is created due to cone movement. The additional flow is induced due to the pressure difference between the inside and outside of the drill string. Important is that the added flow is maximized while the pressure losses due to this flow are minimized. The resulting increased flow through the nozzle decrease the required flow from the top of the bottom hole.

In addition, additional flow is implemented in the numerical model in order to check its applicability. The concept of this mitigation opportunity is a bursting disc with a certain volume of fluid behind it that can be released into the system. If the pressure difference exceeds a threshold pressure, the bursting disc will break and the fluid enters the system at the position of the cone.

4.1. Flow ports

The flow ports are chosen in order to induce flow through the nozzle of the drill string. Due to the equilibrium of the flows at the bottom of the cone, this reduces volume decompression of the bottom hole. The principle of the flow ports is based on the difference between the surge pressure wave moving up in the annulus (red arrows in figure 4.2), and the swab pressure wave moving up in the drill string (blue arrow pointing upward in figure 4.2). This pressure difference, when connected using the flow ports, will induce flow from the high pressure region (annulus) to the low pressure region (inner drill string), and in turn, the region below the cone, see figure 4.3). Concluding, by using flow ports, additional flow from the annulus is allowed through the drill string to fill up the void below the cone.

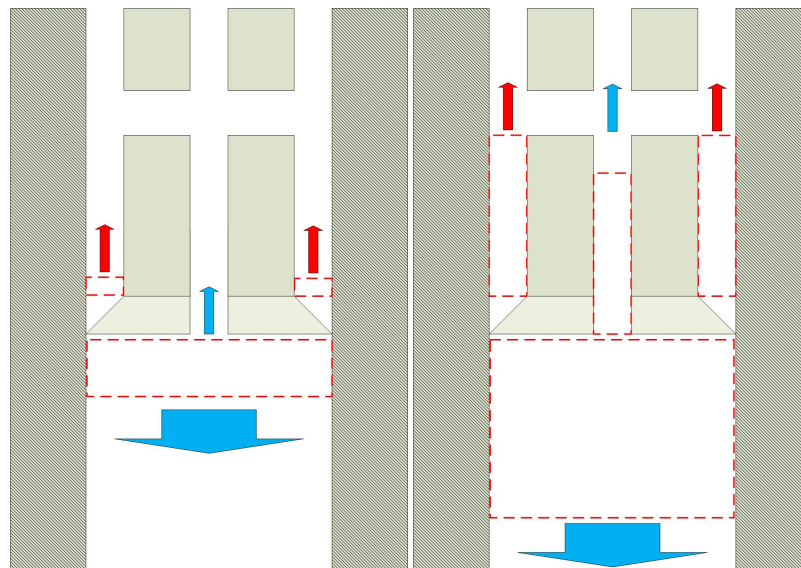


Figure 4.2: Pressure wave propagation after pop-out, the pressure waves propagating

Figure 4.2 shows how the pressures in the annulus, drill string, and bottom hole region propagate as an extending wave, reducing the pressures in the bottom hole and drill string and increasing the pressure in the annulus. Figure 4.3 shows how the pressure difference initiates the flow.

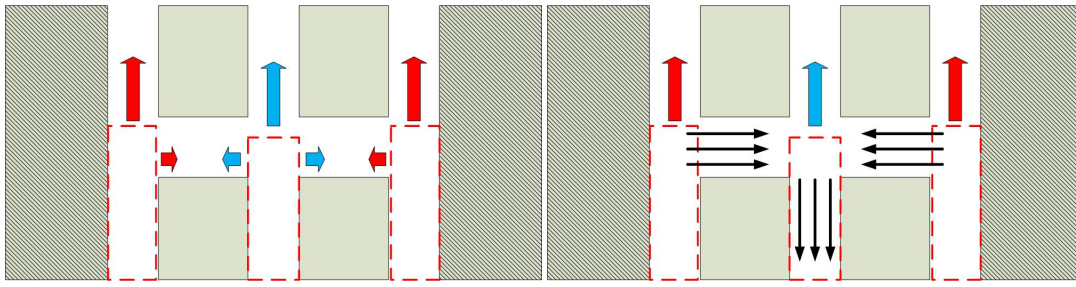


Figure 4.3: Pressure wave propagation after pop-out and the flow that is induced by the pressure difference between the annulus (outer) and inner drill string (black arrows represent the flow direction)

When the waves reach the ports, the pressure difference over the ports will induce flow from the annulus (outer) to the drill string (inner) region. It must be noted that the pressure losses due to this flow (minor losses because of geometry and losses due to change in the direction of the flow) will affect the effectiveness of the flow ports. This has to be taken into account in the design of the flow ports.

4.1.1. Coupling of the annulus and drill string systems

The flow ports have been added to the numerical model by super positioning. For every time step the system is solved with by the original governing equations. Then a set of 3 nodes in the annulus and 3 nodes in the inner drill string and an additional node to determine the velocity and pressure in the flow port are recalculated using the coupled boundary conditions of the flow ports. The mass balances over the volume, Bernoulli equations for unsteady flow for incompressible fluids, and the negative (C-) and positive (C+) characteristic lines on the boundaries are used to solve for these seven nodes, see figure 4.2.

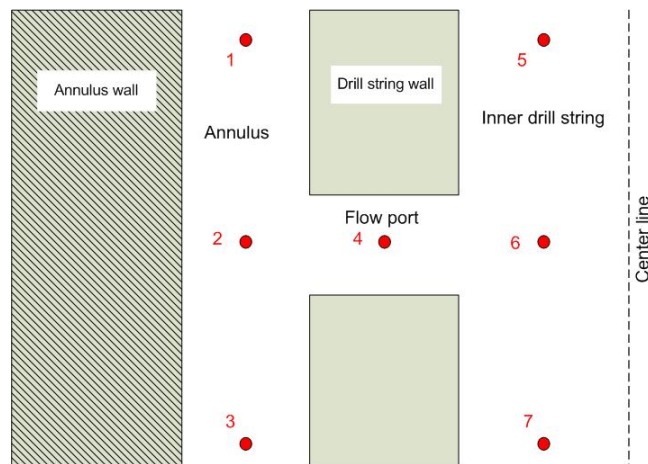


Figure 4.4: Overview of the nodes that are recalculated using the flow port boundary conditions.

The mass balances over the control volume are:

$$A_{ann}v_1 - A_{flowport}v_{flowport} = A_{ann}v_3 \quad (4.1)$$

$$A_{ds}v_7 = A_{ds}v_5 + A_{flowport}v_{flowport} \quad (4.2)$$

The annulus and drill string systems are coupled with the use of a ghost node, node 4, see figure 4.4. This node carries the pressure and velocity information of the flow port. With the use of Bernoulli's equation for unsteady incompressible flow, the drill string is coupled to the annulus. The ports are modelled as branched flows along the same streamline, as done in (Bürmann, 1974) [12]. Figure 4.5 displays how these flows are then coupled by using the information in the ghost node.

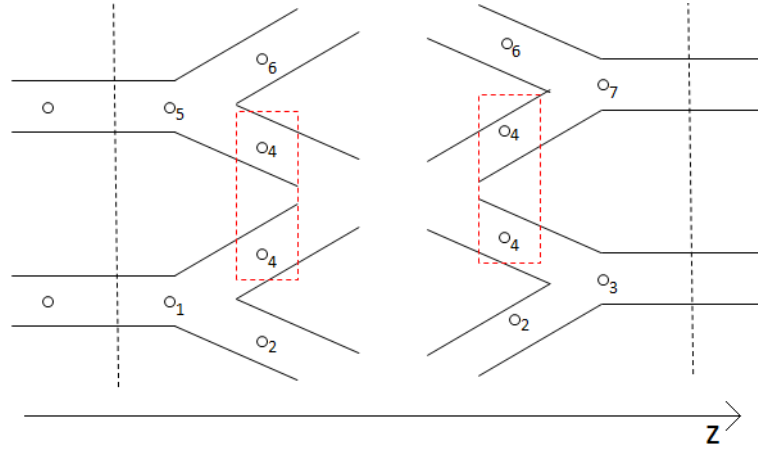


Figure 4.5: Flow port flow as coupled branched flow

The important assumption in this case is that the flow is in the same streamline, therefore we derive the flows in the flow port also as a flow along the z -axis. Because the drill string and the annulus system are modelled only along the z -axis, there is no need to add a dimension in these systems. This way, the numerical model remains one-dimensional (1D). For 1D, the Bernoulli equation for unsteady incompressible flow according to Battjes (1986) is [13]:

$$\nabla \left(\frac{\partial \phi}{\partial t} + \frac{1}{2} |\nabla \phi|^2 + \frac{p}{\rho} + gz \right) = 0 \quad (4.3)$$

Use $\underline{v} = \nabla \phi$:

$$\frac{\partial v}{\partial t} + \nabla \frac{1}{2} |\underline{v}|^2 + \nabla \frac{p}{\rho} + \nabla gz = 0 \quad (4.4)$$

Only z -direction is considered, and using the simplification of the branched flow above:

$$\frac{\partial v_z}{\partial t} + \frac{\partial (\frac{1}{2} v_z^2)}{\partial z} + \frac{1}{\rho} \frac{\partial p}{\partial z} + \frac{\partial gz}{\partial z} = 0 \quad (4.5)$$

Integrate over z :

$$\int_{z_1}^{z_2} \frac{\partial v_z}{\partial t} dz + \frac{1}{2} v_z^2 + \frac{1}{\rho} p \Big|_{z_1}^{z_2} + g(z_2 - z_1) = 0 \quad (4.6)$$

The density is considered constant over the depth of the well. Multiplying with ρ , and rewriting gives:

$$p_1 + \frac{1}{2} \rho v_{z,1}^2 + \rho g z_1 = p_2 + \frac{1}{2} \rho v_{z,2}^2 + \rho g z_2 + \rho \int_{z_1}^{z_2} \frac{\partial v_z}{\partial t} dz \quad (4.7)$$

The term $\int_{z_1}^{z_2} \frac{\partial v}{\partial t} dz$ is the partial derivative of the velocity in time integrated over the distance between point z_1 and z_2 . Numerically, the trapezoidal rule for approximation of the integral [14] combined with the upwind method for the partial derivative [15] can be used to rewrite this term to:

$$\int_{z_1}^{z_2} \frac{\partial v_z}{\partial t} dz \approx \frac{z_1 - z_2}{2} \left\{ \left(\frac{v_2^{t+\Delta t} - v_2^t}{\Delta t} \right) + \left(\frac{v_1^{t+\Delta t} - v_1^t}{\Delta t} \right) \right\} \quad (4.8)$$

In this case the partial derivative in time is assumed to be over t to $t + \Delta t$. This formula is used between all the nodes in figure 4.5. Together with the mass balances described in equation 4.1 and 4.2, the set of nodes is solved to couple the annulus and drill string systems. In order to account for the losses due to the geometry of the flow ports, loss factors have been added to this equation. The next section will describe how the loss factors are determined.

4.1.2. Pressure losses due to ports

The Borda-Carnot equations for sudden contraction and expansion are used to determine the inflow and outflow losses of the flow ports[16] [17].

sudden contraction
$$K_{SC} = \frac{1}{2} \left(1 - \frac{A_S}{A_L} \right)^{\frac{3}{4}} \tag{4.9}$$

sudden expansion
$$K_{SE} = \left(1 - \frac{A_S}{A_L} \right)^2 \tag{4.10}$$

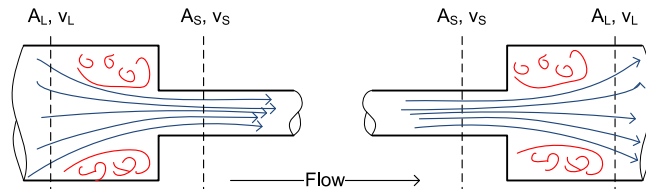


Figure 4.6: Sudden contraction (a) and sudden expansion (b) in a pipe

Where K_{SC} = loss coefficient for sudden contraction; K_{SE} = loss coefficient for sudden expansion; A_S = cross-sectional area for the smaller pipe; and A_L = cross-sectional area for larger pipe as shown in figure 4.6. The coefficients range between 0 and 1. The loss factor is calculated per flow ports. The important dimensions are the thickness of the clearance and the diameter of the flow ports and the drill string. In order to calculate the loss factor, these values are used for the calculation of the ratio between the flow port and clearance, and the flow port and the drill string, see figure 4.7.

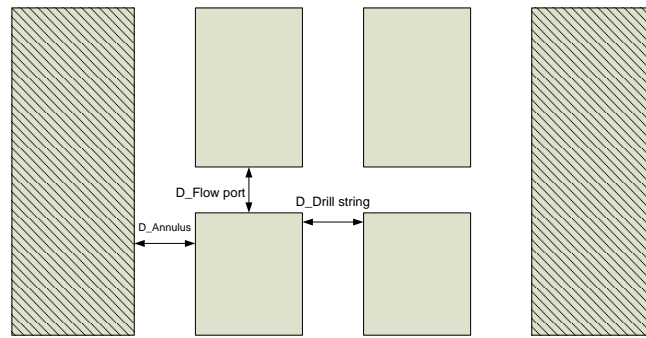


Figure 4.7: The effective diameters for calculation of the loss factors due to expansion and contraction

In addition, due to the 90 degrees directional change of the flow through a branch, theory on fluid flow in T-junctions of pipes [18] is used to account for the branched flow of the flow ports. The loss factor for branched flow in T-junctions is equal to 1 for pipes without a threaded connection, making the total loss factors for the flow ports:

Loss factor flow from annulus into flow port
$$K_{ann} = 1 + \frac{1}{2} \left(1 - \frac{D_{flowport}}{D_{ann}} \right)^{\frac{3}{4}} \tag{4.11}$$

Loss factor flow from flow port into inner drill string
$$K_{ds} = 1 + \left(1 - \frac{D_{flowport}}{D_{ds}} \right)^2 \tag{4.12}$$

It is assumed that these equations approximate the loss factors for the flow ports, but in order to check this it is advised to perform Computational Fluid Dynamics (CFD) calculations on the design of the flow ports for different diameters. Also, the combined flows within the drill string may affect the total loss factor for this geometry. Additionally, sudden contraction and expansion are used where more gradual designs could improve the function of the flow port. This is advised to take into account in the design of the flow ports.

4.2. Additional flow

Additional flow might be possible when a volume of fluid can be introduced into the system. The idea of a stored fluid behind a bursting disc is used. The disc will burst when a pressure difference over the disc exceeds a threshold pressure. The flow released will have an effect on reducing the swab pressure if it can decrease the necessary flow from the bottom hole as discussed earlier in this chapter. This mitigation opportunity is researched in order to predict the amount of flow necessary to significantly reduce swab pressures. When the minimum amount of flow necessary to reduce the swab pressure to a value below the collapse pressure of the pipe is estimated, implementation can be worked out. In this section it is described how the flow is added in the numerical models. In the next chapter, the results of the additional flow are discussed.

4.2.1. Implementation

The additional flow is modelled as an increase in nozzle flow, with the effect that the flow from the top of the bottom hole is decreased. This flow is constant and has a given duration. In addition, an activation method was introduced so that the flow is triggered by the behaviour of the original system. Given these conditions, the flow introduced in the system has several factors that can be influenced:

- Flow rate
- Duration of the flow
- Initiation of the flow

For a realistic implementation of the additional flow, a trigger is defined in order for this flow to start. The pop-out induces a pressure difference in the well, and this difference can be used to trigger the flow. In the design this could be for example a bursting disc that will break due to a pressure difference. The value of the pressure difference required to trigger the flow has an influence on the effectiveness of this mitigation opportunity. This value will be referred to as the *threshold* pressure. Numerically, the additional flow is added into the boundary conditions at the cone.

4.2.2. Numerical implementation

The additional flow is numerically implemented as a simple addition into the existing models. This is done in order to quickly check the applicability of this mitigation opportunity. The flow has been added in the following way:

$$P_{swab} = \frac{-p3_{i-1,1} + L_{upper} * \rho_w * g}{1e5}; \quad (4.13)$$

IF

$$P_{swab} < threshold \quad (4.14)$$

$$Q_{af} = 0; \quad (4.15)$$

ELSE

IF

$$i > time \quad (4.16)$$

$$Q_{af} = 0 \quad (4.17)$$

ELSE

$$Q_{af} = flow \quad (4.18)$$

END

END

Where P_{swab} is the swab pressure at the location underneath the cone, i.e. the pressure difference between the negative pressure wave and the hydrostatic pressure at that location. Q_{af} is the added flow. The input variables are the 'flow' (flow rate), 'time' (duration), and 'threshold' (differential pressure to initiate the flow).

The flow is then implemented in the boundary conditions at the as:

$$v_n = v_n - \frac{Q_{af}}{A_n} \quad (4.19)$$

$$v_3 = v_3 - \frac{Q_{af}}{A_3} \quad (4.20)$$

Where v_n is the nozzle flow velocity, A_n is the nozzle area, v_3 is the velocity of the flow from the bottom hole, and A_3 is the bottom hole area. The additional flow is deducted from both variables because the values for nozzle velocity are positive (for downwards flow into the void underneath the cone) and the values for bottom hole velocity are negative (for upwards flow into the void).

5

Results

This chapter describes the results obtained from the numerical implementation of the mitigation opportunities introduced in the previous chapter. The effect these opportunities have on the swab pressure is important to determine the applicability of both options. First the results from the flow port implementation will be discussed and after the results from the additional flow opportunity.

5.1. Flow ports

The implementation of the flow ports has been done in the models of Van Dongen and Tillema [3] [4]. The base case of the flow port implementation consists of the settings found in table 5.1.

Table 5.1: Base case settings for the flow port implementation

Parameter	value	unit	value	unit
Host pipe inner diameter	10.2	["]	259.08	[mm]
Cone outer diameter	10.0	["]	254	[mm]
Expansion force	216	[mT]	2119	[kN]
Distance to the cone	4	[m]		
Flow port diameter	1	["]	25.4	[mm]
Number of flow ports	4	[-]		
Length of gradual decrease expansion force	0.3	[m]		
Reflection	1	[-]		

The factors influencing the flow ports are the distance to the cone, the flow port diameter and the number of flow ports. The settings mentioned in the table are the standard settings by which the results will be described. Later in this chapter a sensitivity analysis discusses the factors that are influenced by the flow ports (distance to the cone, flow port diameter, and number of flow ports). The clearance is the difference between the host pipe ID and cone OD and cannot be changed. Furthermore, the length of gradual decrease of the expansion force takes into account a decreasing contact area between the cone and the liner when the cone exits the liner. This parameter cannot be changed because it is dependent on the size of the cone. Finally, full reflection is assumed for conservative reasons. The reflection factor is unknown, but very hard rock can be present in the well, thereby creating large reflection coefficients.

5.1.1. Results

In this section the numerical results for the integration of the flow ports will be discussed. The flow rates of the different fluid areas are discussed in order to verify the implementation of the flow ports. The pressures at the bottom of the hole and halfway the bottom hole region are displayed in order to verify the effect of the mitigation opportunities.

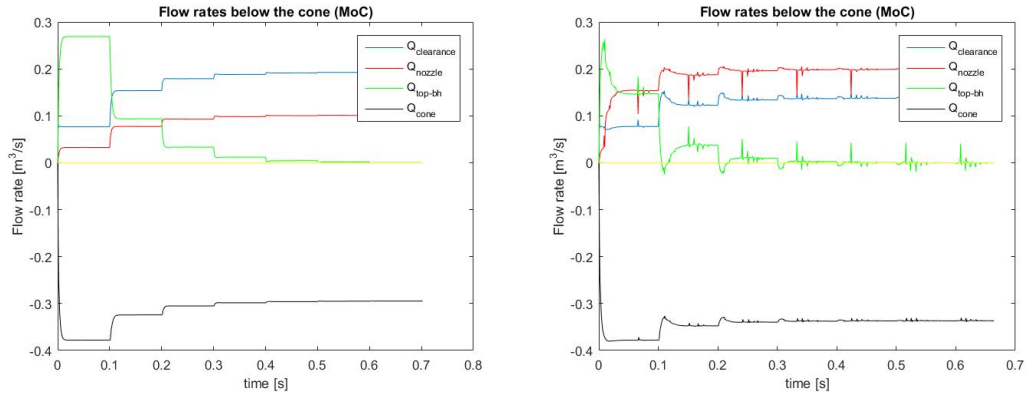


Figure 5.1: Flow rates without (left) and with (right) flow ports.

The flow rates of the model without the flow ports is displayed on the left and shows a clean development of flows over the time. On the right the flow rates of the model including the flow port implementation are displayed. The most important difference is the drop in flow from the top of the bottom hole (the green line in the figures) in the first 0.1s. This drop is associated with the rise in the nozzle flow, because the flow ports increase the flow through the nozzle and thereby decrease the flow required from the top of the bottom hole. The increasing number of peaks in the flow port models are due to the reflections of the pressure waves between the upside of the cone and the interface between the nozzle and the bottom hole areas. Changes in material and flow area cause reflections of the pressure waves, and every time there is a pressure difference over the ports, the flow through the flow ports is increased or decreased. Due to the decrease of flow from the top of the bottom hole, the decompression of this region should decrease as well. Later in this chapter the results for the pressure development over time will be discussed.

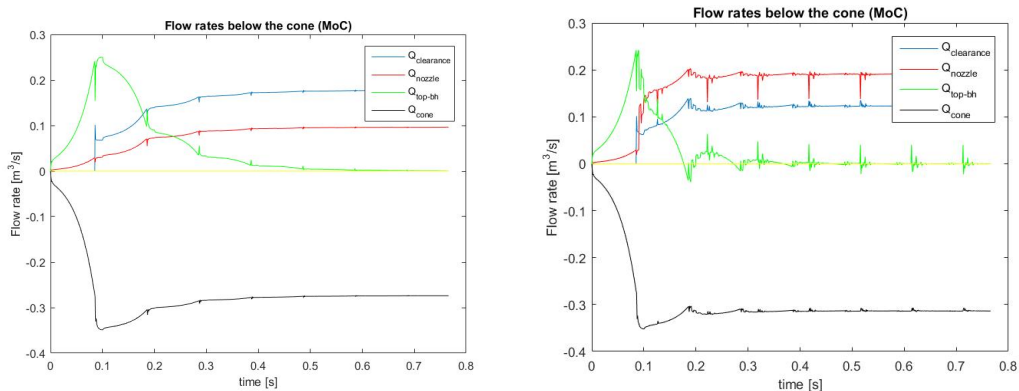


Figure 5.2: Flow rates without (left) and with (right) flow ports with a gradual decrease in expansion force.

The models including the gradual decrease of expansion force show similar behaviour as the standard model, see figure 5.2. But, in these models, it can be seen that the flow from the top of the bottom hole is not instantly increased in the first moments, but a more gradual decrease is noticed. The effect of the flow port is similar in the flow rates for both models, verifying that the implementation is done equally.

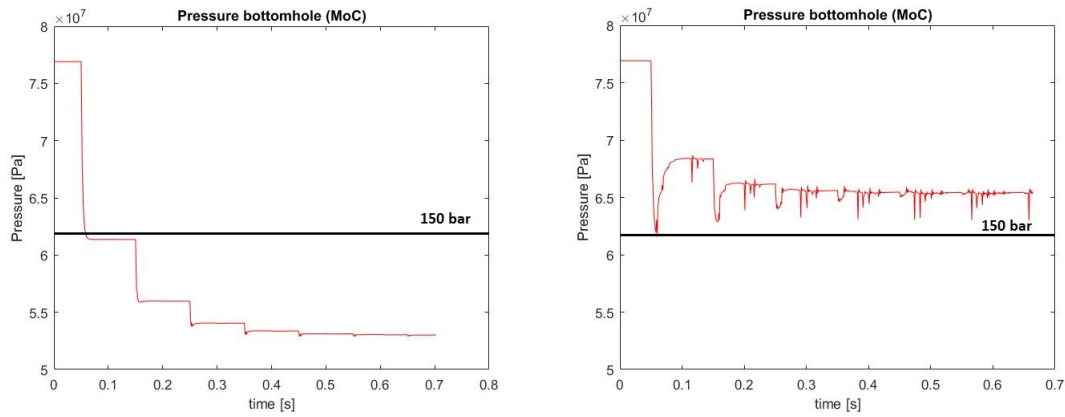


Figure 5.3: Pressure at the bottom without (left) and with (right) flow ports. The 150 bar line represents the 150 bar swab pressure that may not be exceeded.

The graphs in figure 5.3 show the pressure over the time in the standard numerical model and the model with the flow port implementation. In the normal model only the swab pressure wave is displayed and the reflections at the bottom of the hole can be seen. The reflections are the vertical drops in pressure in the graph. In the model without flow ports, the pressure only experiences decreases and reaches a steady-state pressure of approximately 530 bar, resulting in a swab pressure of 250 bar.

In the model with flow ports, two important differences can be seen. After every pressure drop there is a gradual increase in pressure. This increase is the contribution of the flow from the flow ports that cause the decompression of the region below the cone to decrease; this flow is seen in figure 5.1. The other difference is that the resulting steady-state pressure is above the 150 bar swab pressure limit (for pipe collapse). This means that in the current configuration, the flow ports have a significant effect on the swab pressure, and that pipe collapse could be prevented. It is important to note that the swab pressure does exceed the limit for about 1 ms during the first pressure drop. It appears that in the numerical model, the flow ports show promising behaviour of successfully mitigating the swab pressure problem.

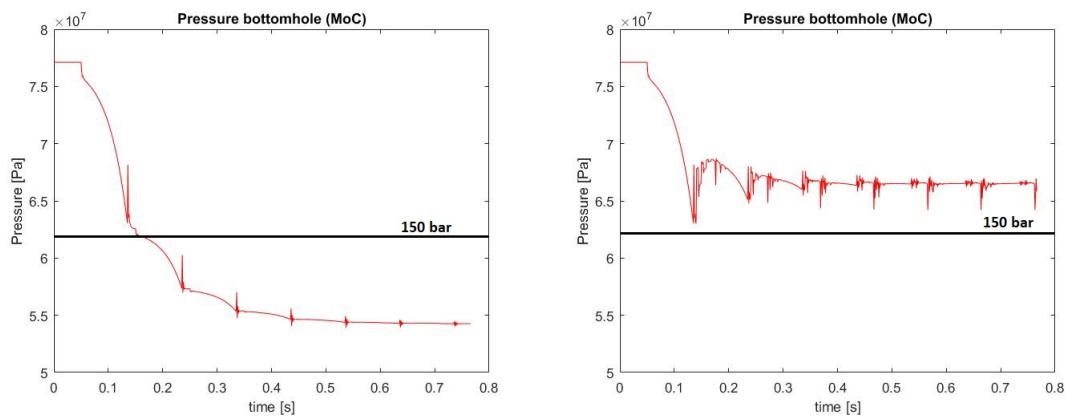


Figure 5.4: Pressure without (left) and with (right) flow ports with a gradual decrease in expansion force.

In the graphs in figure 5.4 the pressure over time is displayed for the model including the gradual decrease in expansion force. The graph on the right displays the flow port implementation in this model. The pressure development of the flow port model is similar as the normal model. This is expected in the analysis of the flow rates. Also in this configuration and using the model with a gradual decrease in expansion force, the pressure in the bottom hole stay above the limit of 150 bar swab pressure. This means that also this numerical implementation shows promising behaviour of the flow ports.

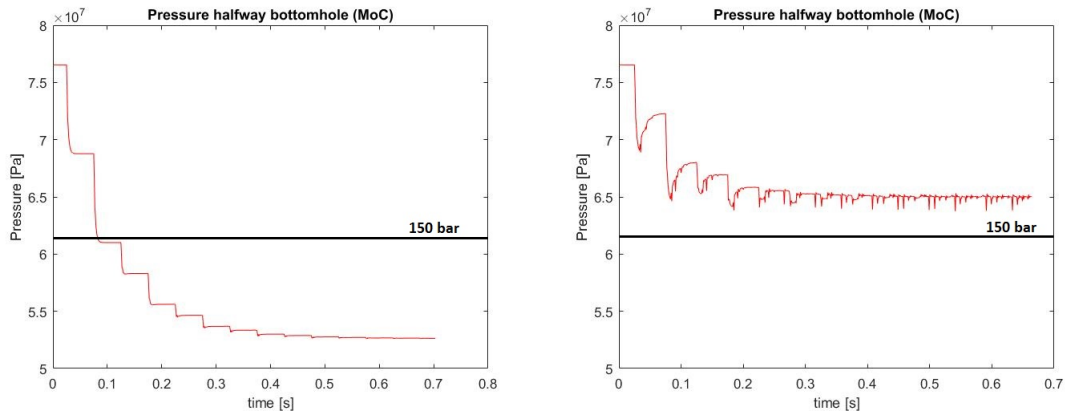


Figure 5.5: Pressure without (left) and with (right) flow ports.

The casing is supported by the overlap section at the top and by open hole anchors in the bottom of the well during pipe expansion. Therefore, halfway the bottom hole region the pipe is the weakest because it has no additional support next to the formation and is furthest away from the support. The pressure halfway the bottom hole is for that reason the most dangerous for pipe collapse. In order to investigate the pressures at this location the graphs in figures 5.5 and 5.6 have been plotted. The most important difference is the number of pressure drops. The number of drops is twice that of the previous plots because at the bottom of the hole, the pressure wave is reflected and doubles amplitude. The initial pressure drop is for that reason also half of that of the previous graphs.

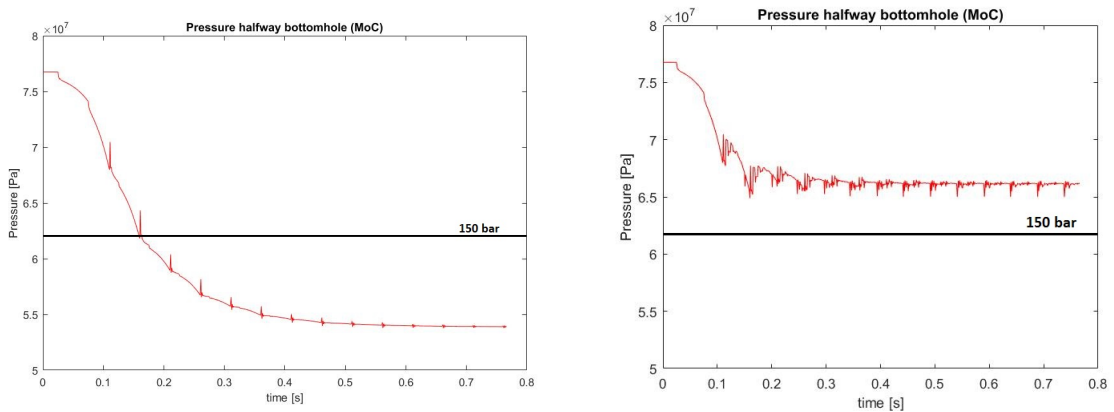


Figure 5.6: Pressure halfway the bottom hole without (left) and with (right) flow ports with a gradual decrease in expansion force.

5.1.2. Sensitivity analyses

A sensitivity analysis has been performed to verify the function of the flow ports and to determine the parameters that most influence the swab pressure. The analyses have been performed on both numerical models. The parameters that are analyzed can be found in table 5.2. The sensitivity is researched for values of 50% and 150% of the base case, because in this configuration the number of flow ports remains an even number. An even number of flow ports is desired because the flows through the ports into the inner drill string will be symmetric. This will prevent effects of the symmetry of the flow into the drill string to influence the analysis. The flow port diameter has a direct effect on the loss factors for the flow ports. The ratios between the effective diameter and the associated loss factors can be found in table 5.3.

Table 5.2: Values of parameters used in sensitivity analysis for flow ports

Parameter	50%	100%	150%
Distance to cone [m]	2	4	6
Flow port diameter ["]	0.5	1	1.5
Number of flow ports [-]	2	4	6

Table 5.3: Area ratios for the pressure loss factor

Diameter of flow port	0.5"	1.0"	1.5"
$D_{flowport}/D_{clearance}$ [-]	0.175	0.351	0.526
Contraction loss factor per flow port [-]	0.4327	0.3616	0.2855
$D_{flowport}/D_{drillstring}$ [-]	0.137	0.275	0.412
Expansion loss factor per flow port [-]	0.7441	0.5260	0.3456
Total loss factor per port [-]	3.1768	2.8876	2.631

In the tornado charts in figure 5.7, the red bars represent the parameters with a value of 150% of the base case values and the blue bars represent the parameters with a value of 50% of the base case values. The sensitivity analysis shows that the flow port diameter has the largest effect on the swab pressure, the number of ports has a smaller effect on the swab pressure and the distance to the cone has no effect on the swab pressure.

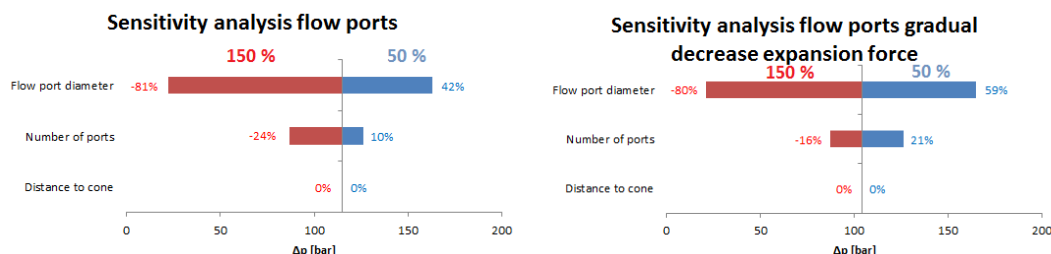


Figure 5.7: Tornado charts of parametric study of flow ports for steady-state pressure.

Distance to the cone

The distance to the cone did not show any effect on the steady-state swab pressure. It is interesting to see if this parameter can have effect (for longer distances) on the swab pressures, in case the implementation of the flow ports has to be placed further away from the cone for any reason. For that reason, the effect has been researched if the flow ports were placed 100, 200, and 300 meters away from the cone. The graphs in figure 5.8 display these effects, d represents the distance between the flow ports and the cone.

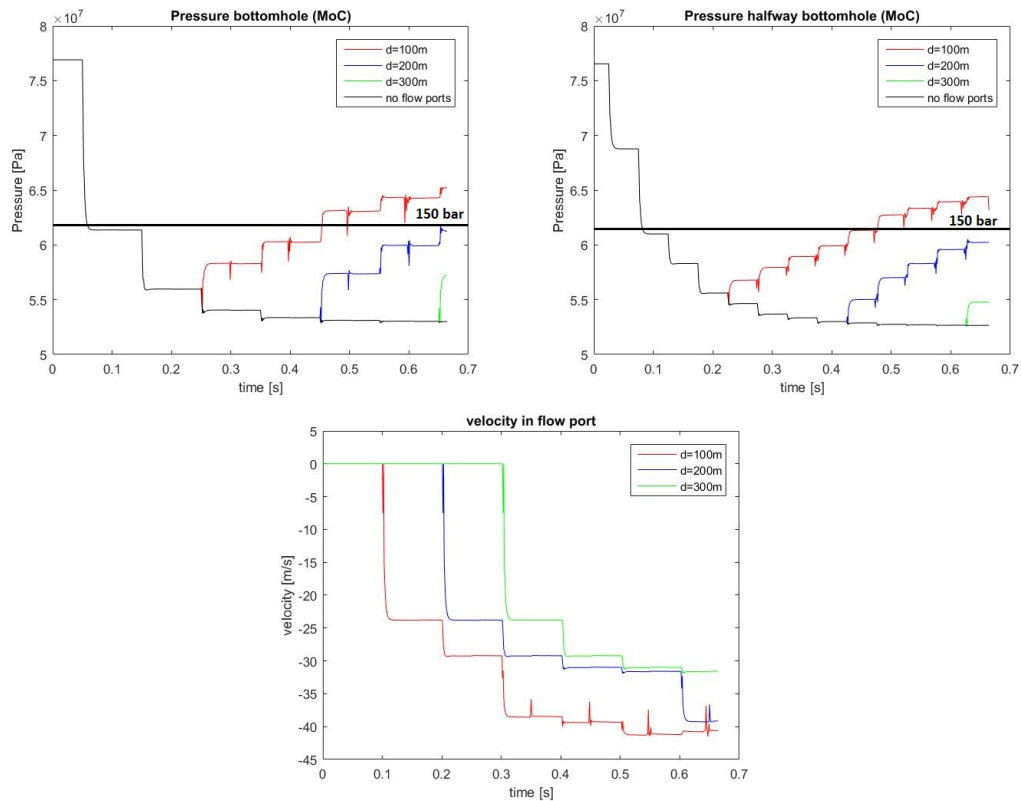


Figure 5.8: The pressure at the bottom hole and halfway the bottom hole region, and the velocity in the flow ports for the far placement of the flow ports.

The graphs show the effect of the placement of the flow ports. In all situations the pressure reaches levels beyond the 150 bar swab pressure limit. But the distance to the cone influences the time it takes before the effect of the flow port is visible. It takes 228, 428, and 628 milliseconds for the ports to show effect for 100, 200, and 300 meter placements away from the cone. It can be deduced that it takes 28 milliseconds for the flow to develop and for every 100 meters distance from the cone a total delay of 200 milliseconds should be taken into account. The speed of sound in the mud is 1000 m/s and the distance is 100m, therefore 100ms are necessary to reach the ports and the same amount of time is necessary to travel back to the the cone.

Flow port diameter

The flow port diameter was found to have the most influence of the swab pressure. The graphs in figure 5.9 show the difference in the pressure development at the bottom of the hole for the three diameter configurations examined: 0.5, 1.0, and 1.5 inch. The 1.0 and 1.5 inch flow port models show that with the configuration used - 4 flow ports, 4 meters away from the cone - the flow ports will increase the steady-state pressure in the well and reduce the swab pressure until under the collapse value of 150 bar.

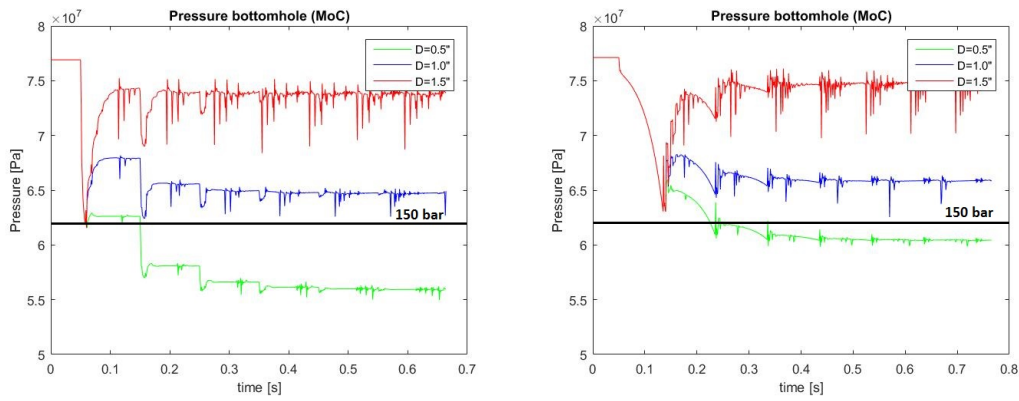


Figure 5.9: The effect of the diameter change of the flow ports for the normal model (left) and the model with gradual decrease of expansion force (right).

Pressure loss coefficient

In chapter 4 the pressure loss coefficient is calculated to take into account the area change and direction change of the flow. Because this resulting coefficient is an assumption, a sensitivity analysis on the effect of the loss coefficient is performed. The pressure loss coefficient for the flow ports has been changed to 80% and 120% of its original value. The results can be seen in figure 5.10 and in table 5.4. In both models, a 20% higher pressure loss coefficient causes a 6% higher swab pressure and a 20% lower pressure loss coefficient causes a 8% lower swab pressure.

Table 5.4: Influence of the pressure loss coefficient on the swab pressure

Parameter	k80%	k100%	k120%
Normal model: swab pressure [bar]	106	115	122
Percentage change	-8%	-	+6%
Gradual decrease expansion force: swab pressure [bar]	97.3	106	113
Percentage change	-8%	-	+6%

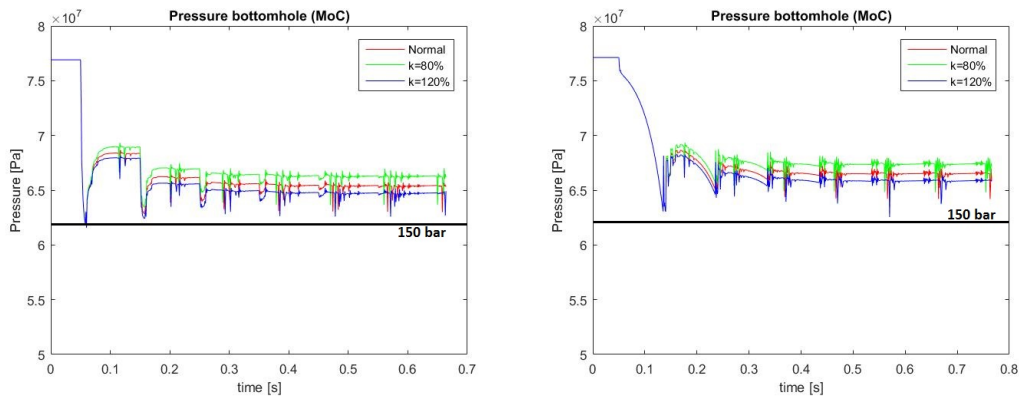


Figure 5.10: Sensitivity of the pressure loss coefficient, k, for the normal model (left) and the model with gradual decrease of expansion force (right).

5.2. Additional flow

The goal of the additional flow implementation is to decrease the swab pressure below 150 bar and to check how much volume of fluid is required. The concept of the additional flow works as follows: normal cone pop-out occurs, when the difference between the pressure below the cone and the hydrostatic pressure is larger than the *threshold pressure*, a bursting disc bursts and the flow initiates (the time it takes for the burst disc to burst has not been taken into account). The flow will have a certain flow rate and will end after a certain duration. The parameters affecting the additional flow method are described in table 5.5. The duration of the flow combined with the flow rate determine the total volume required. The base case has been chosen as a flow rate of $0.1 \text{ m}^3/\text{s}$ with a duration of 0.1 s, resulting in a volume of 10 litres. This is almost twice the volume of the cone (a 10.0" cone has a volume of around 5.3 litres), but for lower volumes results were not visible.

Table 5.5: Base case settings for the additional flow implementation

Parameter	value	unit	value	unit
Host pipe inner diameter	10.2	["]	259.08	[mm]
Cone outer diameter	10.0	["]	254	[mm]
Expansion force	216	[mT]	2119	[kN]
Flow rate	0.1	$[\text{m}^3/\text{s}]$	100	L/s
Duration of flow	0.1	[s]	100	[ms]
Threshold pressure	40	[bar]		
Total volume required	0.01	$[\text{m}^3]$	10	[L]

5.2.1. Results

The additional flow has been modelled for four cases, ranking from low to high. The graphs for these cases are displayed in figure 5.11 for the pressures bottom hole and for the pressure halfway the bottom hole region. The values used for the cases are given in table 5.6. The values are only changed from the base case values for the parameter given in the legend of the graph.

Table 5.6: Values of parameters used in sensitivity analysis for additional flow

Parameter	unit	low	base case	high	highest
Flow rate	$[\text{m}^3/\text{s}]$	0.05	0.10	0.15	0.20
Duration of flow	[ms]	50	100	150	200
Pressure required to initiate flow	[bar]	20	40	60	80

The graphs show the effect per parameter, while the other parameters stay on the base case level. This gives volumes that range between 5 to 20 litres of fluid. The effect of each of the parameters can be seen in the graphs in figure 5.11. Each parameter will be discussed shortly in the following sections.

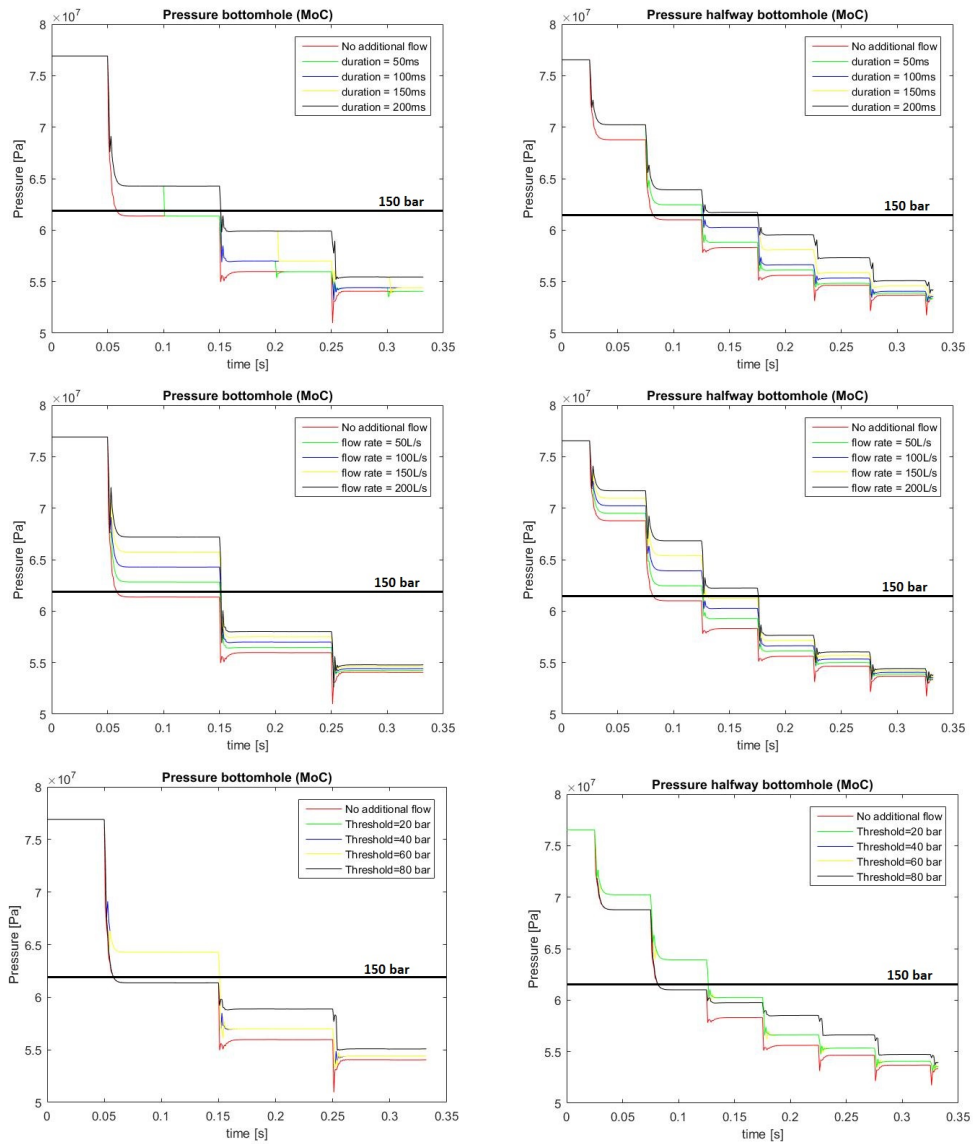


Figure 5.11: Pressures at the bottom of the hole (left) and halfway the bottom hole (right) for different durations (up), flow rates (middle), and threshold pressures (bottom).

Duration of flow

The duration of the flow influences when the pressure starts to drop again. Longer durations also have the effect that the steady-state pressure is higher and therefore the steady-state swab pressure is reduced. The reduction of the swab pressure in with the largest time time frame of 200 ms is 14 bar (or 2.5%).

Flow rate

The effect of the change in flow rate is mostly seen in the reduction of the first pressure drop. This can be explained by the flow rates in figure 5.1, because the flow rate added directly reduces the contribution of the flow from the top of the bottom hole, this is the expansion of this region that causes the decompression. The steady-state swab pressure reduction is 6 bar (or 1%) and therefore this has no significant effect on the swab pressure. The effect on the first pressure wave is interesting, if this mitigation opportunity is used in combination with the flow ports. In figure 5.12 it can be seen that the effect of the flow rate on the reduction of the swab pressure is linear. The volumes associated with the flow rates are as such: for a $0.2 \text{ m}^3/\text{s}$ flow rate and a duration of 0.1 s, the volume is 20 L.

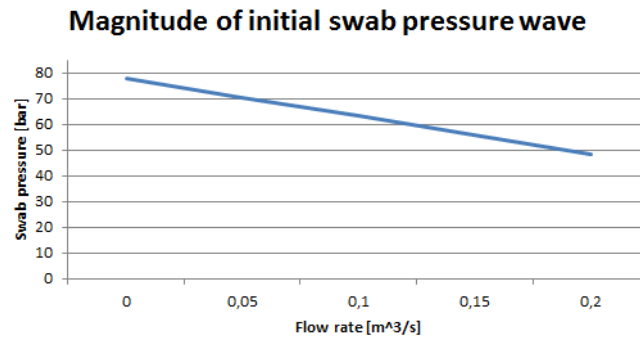


Figure 5.12: Effect of flow rate on the magnitude of the initial pressure wave.

Threshold pressure

The threshold pressure, or the pressure required to initiate the additional flow, the bottom graphs in figure 5.11, influences the moment in time the flow is initiated. It can be seen that the flows for threshold pressures lower than 80 bar are all initiated due to the first pressure wave and for that reason these configurations also have an effect on this wave. For the plot with a threshold pressure higher than 80 bar it is clear that the flow will be initiated after the first pressure wave is reflected at the bottom of the hole and reaches the cone. For the additional flow to be more effective it is important that the threshold pressure is set to a lower value than 80 bar. In turn, the bursting disc as suggested in chapter 4 must break within milliseconds in order to have effect on the initial pressure wave. The effect on the steady-state pressure in this time frame is 10 bar (or 2%) and is not significant in order to reduce swab pressures.

5.3. Discussion

In this chapter the results from the two mitigation opportunities have been discussed. The flow port implementation shows very promising results, significantly reducing swab pressures. The sensitivity analysis performed on the parameters affecting the swab pressure shows that the diameter of the flow ports has the largest influence on the swab pressure. With a diameter of 1" the flow ports significantly reduce swab pressures (using 4 ports at 4 meters away from the cone). The pressure loss coefficient (k-factor) that has been assumed in chapter 4 was also researched on sensitivity and for 20% difference in k-factor the swab pressures change between 8% reduction and 6% increase, for lower and higher k-factors respectively. The additional flow opportunity has been researched and for volumes until 20 litres, almost 4 times the volume of the cone, no significant reductions of the steady-state swab pressure are possible. The additional flow opportunity can decrease the initial pressure wave, but only if the initiation of this flow is instantly as is assumed in these models. The applicability of a bursting disc must be researched further (the time it takes for the disc to burst is crucial for this method to decrease the initial pressure wave).

6

Conclusion and recommendations

6.1. Conclusion

An experiment setup has been designed in order to validate the effect of four important factors in the cone pop-out process: The force applied on the system to expand the liner (expansion force), the clearance between the outer diameter of the cone and the inner diameter of the host pipe, the geometry of the cone tail, and the properties of the fluid around the cone. This experiment can be executed in the test rig of the Shell Project & Technology Rijswijk facility.

Two opportunities to mitigate the swab pressure problem for a 10.2" host pipe and a 10.0" cone have been researched. Flow ports connecting the annulus region with the inner drill string will induce flow through the drill string to help fill up the void below the cone. Four flow ports with a diameter of 1" placed 4m above the cone show promising behaviour in reducing the steady-state swab pressure in the well. Swab pressures can be lowered to safe values where pipe collapse will not occur. But, the flow ports start working after the cone pop-out occurs. Therefore, the flow ports do not reduce the initial pressure peak due to cone pop-out. This pressure peak is present for a few milliseconds, depending on the distance the flow ports are placed from the cone.

The second mitigation opportunity is an additional flow into the system. A flow is added after the pressure difference between swab pressure and hydrostatic pressure exceeds a threshold value. Flow starts to flow from the cone to the void in order to decrease the bottom hole decompression. The volume required for the additional flow opportunity is large in order to safely reduce the steady-state pressures. Additional flow may decrease the first pressure wave, but the initiation method must be researched. In order for the additional flow to successfully decrease the initial pressure wave, the initiation method, i.e. the bursting discs must break within a few milliseconds before the swab pressure has fully developed. The time it takes for the initiation method to work affects the size and duration of the first pressure peak.

The sensitivity analysis performed on the parameters influencing the flow ports shows that the flow port diameter has a large influence on the effectiveness of this mitigation opportunity. The diameter of the flow port also affects the loss factors used for the inflow into the port and the outflow into the drill string. The sensitivity analysis performed on the assumed loss factor shows that the loss factor influences the swab pressure and therefore has to be researched.

6.2. Recommendations

The first recommendation is that the numerical model has to be validated through experiments. At this moment the theoretical working of the phenomenon has been researched extensively, but experimental validation remains important.

Secondly, the flow ports show opportunities to significantly reduce the swab pressure. But, assumptions have been made considering the loss factors that have to be validated. The loss factor of the flow ports is recommended to determine with three-dimensional Computational Fluid Dynamics analyses. In addition, it is recommended to inspect the design of the cone and drill string and search for the smallest possible distance between cone and flow ports, because this has an influence of the duration of the initial pressure peak.

Third, the time it takes for a liner to collapse has not yet been researched and can be very interesting. In case the casing can hold during such a short period, the flow port concept can be defined as a working solution to the swab pressure problem. But also, research should be done to verify the peak pressures cylindrical pipes can sustain for duration and magnitude of the peaks. This is important to determine the working envelope for MOD.

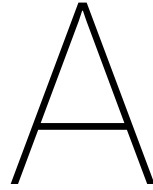
Fourth, the additional flow implementation has been researched for a base case and some variations, but has not been optimized. It is interesting to research the minimal duration and maximal flow rates possible for the additional flow, in order to obtain the optimal volume for this implementation.

Fifth, the additional flow mitigation opportunity shows applicability in order to reduce the initial pressure wave due to pop-out. However, to trigger this flow a bursting disc is suggested. The time it takes for this disc to burst and allow the flow may not be larger than a few milliseconds. It is recommended to research the suggested bursting discs, but also other opportunities for a quick release of the additional flow.

Last, this research assumes full reflection at the bottom of the hole. Reflection factors are not known for different down-hole materials or geometries. Since the reflection factor has a significant influence on the steady-state swab pressure in the hole, it is interesting to research this factor.

Bibliography

- [1] P. Bommer, *A Primer of Oilwell Drilling: A Basic Text of Oil and Gas Drilling*, 7th ed. (Petroleum Extension Service, Continuing & Extended Education, University of Texas at Austin, 2008).
- [2] J. Beckman, *Majors continue to push boundaries of extended-reach drilling*, Offshore (2013).
- [3] J. W. van Dongen, *Swab pressure due to cone pop-out, a numerical approach*, Master's thesis, Delft University of Technology (2015).
- [4] H. A. M. Tillema, *Measuring swab pressure due to cone pop-out, resulting from tubular expansion during Mono diameter drilling*, Master's thesis, Delft University of Technology (2015).
- [5] K. Niemeyer, *Breakthrough in the deep*, Shell IR&D online (2015).
- [6] API, *API Bull 5C3, Bulletin on Formulas and Calculations for Casing, Tubing, Drill Pipe and Line Pipe Properties*, 6th ed. (API, 1994).
- [7] M. Moran, *Fundamentals of Engineering Thermodynamics*, 5th ed. (Wiley, J. & Sons, 2004).
- [8] e. i. c. Lide, D. R., *Handbook of Chemistry and Physics*, 73rd ed. (CRC Press, 1992).
- [9] A. Steel, *17-4 PH data bulletin* (AK Steel, 2007).
- [10] J. W. Hartsuijker, C. & Welleman, *Constructiemechanica 3, Module: Stabiliteit van het evenwicht, Deel 1: Theorie* (TU Delft, 2007).
- [11] Ringfeder, *Standard Friction Springs* (Ringfeder, 2015).
- [12] W. Bürmann, *Drückstosse in koaxialen Rohrsystemen* (Berenz, 1974).
- [13] J. Battjes, *Korte golven* (TU Delft, Section Hydraulic Engineering, 1986).
- [14] J. Van Kan, G. Segal, and F. Vermolen, *Numerical Methods in Scientific Computing*, 2nd ed. (VSSD, 2014).
- [15] C. Vuik and J. Van Kan, *Numerical Methods for Ordinary Differential Equations*, 1st ed. (VSSD, 2007).
- [16] I. Idel'čik and O. Steinberg, *Handbook of Hydraulic Resistance* (Jaico Publishing House, 2005).
- [17] E. Department, *Flow of fluids through valves, fittings, and pipe*, Technical paper (Crane Co., 1988).
- [18] P. R. Vasava, *Fluid Flow in T-Junction of Pipes*, Master's thesis, Lappeenranta University of Technology (2007).
- [19] D. C. Montgomery, *Design and analysis of experiments* (Wiley, J. & Sons, 2008).



Experiment set-up

The experiment set-up including the dimensions is given in figure A.1.

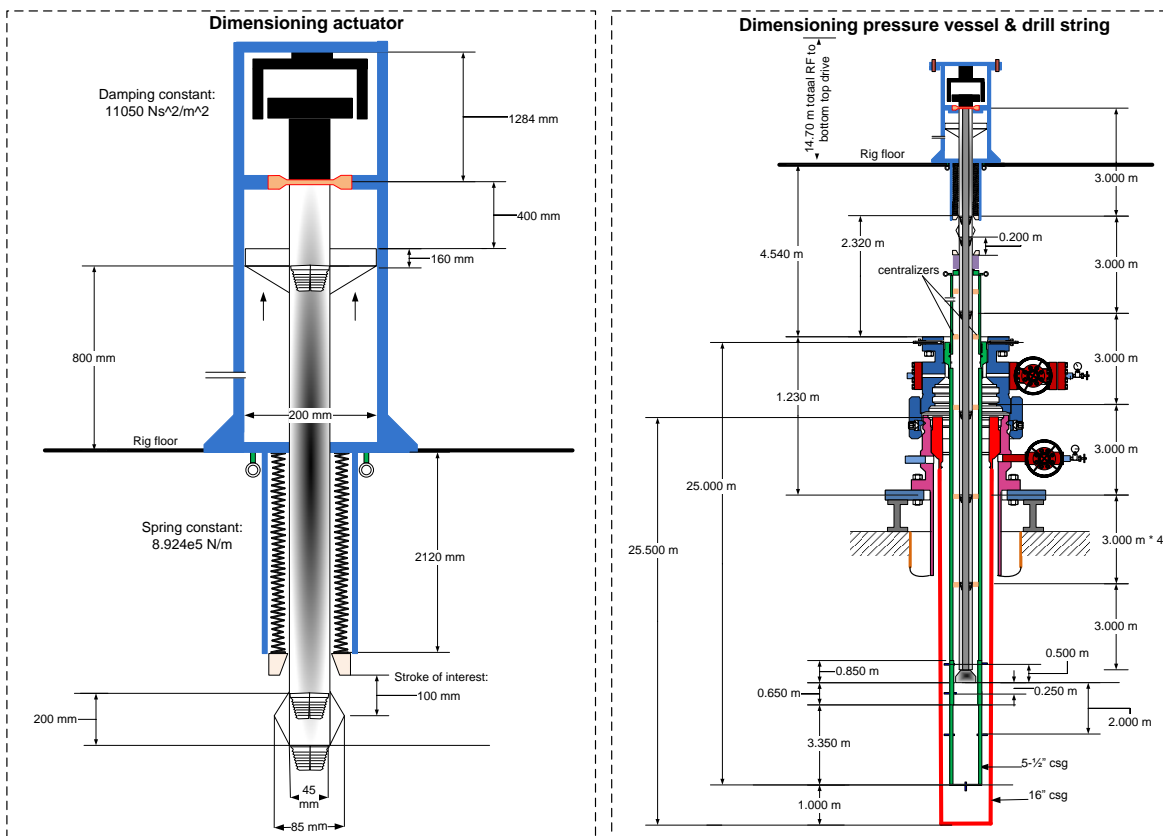


Figure A.1: Dimensions of the actuator (left) and full set-up (right)

Figure A.1 describes all the important dimensions in the actuator (left) and the major dimensions of the set-up (right). This experiment is designed for the test rig in the SPTR facility. The casing hangers visible in the right figure are available at this facility. The dimensions on the left of the right figure display the lengths of casing and space between the ground and rig floor, the dimensions on the right of the right figure display the lengths of drill string. The spacing between the ground and rig floor is specific for this location.

B

Assembly and experiment plan

This appendix describes the assembly, the proceedings between experiments, and the disassembly of the experiment set-up, see figures B.1 to B.7. In addition to these different experiment settings the water in the pressure vessel can be replaced with drilling mud or other fluids in order to check the influence of viscosity on the swab pressures.

In order to statistically have a sound experiment a random order is necessary to minimize the effect of uncontrolled influence on the experiments [19]. The design of this experiment consists of 16 tests in blocks of 4 tests with the same cone. The blocks have been chosen to minimize cone changes, since this takes significantly more time than a shear pin change. If an additional fluid is implemented in the experiment, another 16 runs need to be performed to validate the effect. In table B.1 the design of experiment is given, and the experiment order is suggested in the first column, the cone to be used in the second column, the strength of the shear pin in the third column and the nitrogen pressure to be applied in order to break the shear pin in the last column.

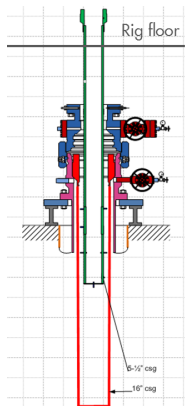
Table B.1: Design of experiment

Experiment number	Cone OD [mm]	Shear pin [mT]	Nitrogen pressure [bar]
1	99.568	27.2	79.9
2	99.568	36.8	111
3	99.568	27.2	79.9
4	99.568	32	95.7
5	101.6 (extended tail)	27.2	79.9
6	101.6 (extended tail)	36.8	111
7	101.6 (extended tail)	32	95.7
8	101.6 (extended tail)	32	95.7
9	101.6	32	95.7
10	101.6	32	95.7
11	101.6	27.2	79.9
12	101.6	36.8	111
13	100.584	36.8	111
14	100.584	27.2	79.9
15	100.584	32	95.7
16	100.584	36.8	111

B.1. Assembly

Assembly step 1:

Make up 5.5" casing using Pallfinger and lift nubbin. Lift bottom of casing above hanger to install cables and protectors. Run down into hole. Make sure cables are intact and casing is not squeezed or deformed, especially at length with thicker wall. To prevent damage and deformation; do not use pipe handler.



Tightening torque:

Casing to host pipe 7000Nm \pm 500 Nm
 Casing 25000 Nm \pm 1000 Nm
 Casing to cross over 7000Nm \pm 500 Nm
 Cross over to liner hanger 4500 \pm 500 Nm

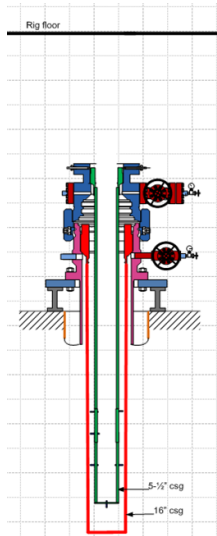
Assembly step 2:

Hang off entire 5.5" casing using top drive and running tool, make sure cabling is run through hanger underneath the no go.

Check the signal in the cable.

Place cover tube

Tightning torque: 37000Nm \pm 1000Nm



Assembly step 3:

Drill string sections are picked up with Pallfinger crane. A lifting clamp has to be placed on the drill string sections.

Make up cone and drill string above rig floor using a hand torque wrench (make-up torque = 700 Nm \pm 200 Nm, dope to be used: Not Prescribed yet).

Connect pre-installed cables, make sure cables are not caught between connection.

Lower with lifting clamp and hang-off on the C-plate (mounting bush small).

Make sure centralizers are not damaged. Check if cable signal is intact with every cable connection.

Cable to be clamped at the connections

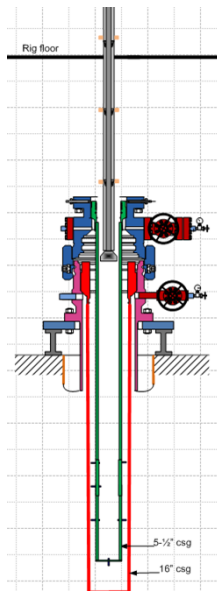
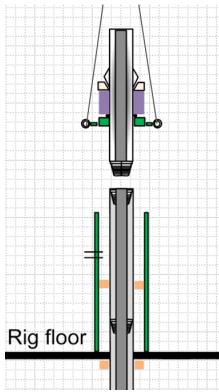
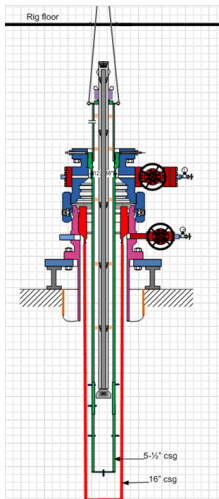


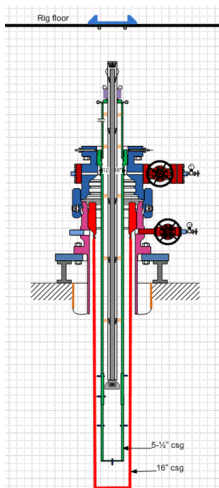
Figure B.1: Assembly step 1,2,3

**Assembly step 4:**

Make up drill string until before bulge joint (donut) above rig floor. Hang off casing using C-plate. Make up donut joint (including top lid) to drill string. Check cable signal. Make sure the drill string sections are secured and can not fall down into the casing.

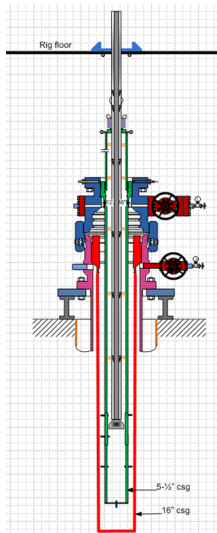
**Assembly step 5:**

Lift plate lid to carry the drill string at the bulge. Release slips and lower top lid and drill string on casing shoulder.

**Assembly step 6:**

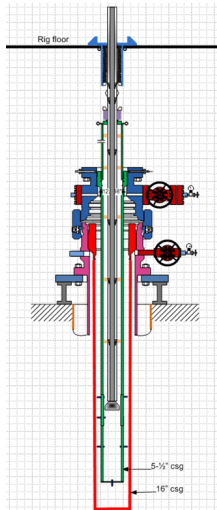
Fix the top lid on the 5.5" casing; tighten the bolts on top. Install ground plate on rig floor and centralize above the casing. Centralize and fix the rig plate.

Figure B.2: Assembly step 4,5,6



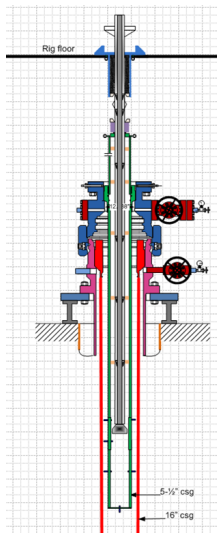
Assembly step 7:

Make up drill string until piston joint. Drill string is supported by the toplid. Check the signal in the cable.



Assembly step 8:

Install spring package over the placed drill string. Make sure spring package is centralized above the drill string and the drill string can move without touching the friction springs.



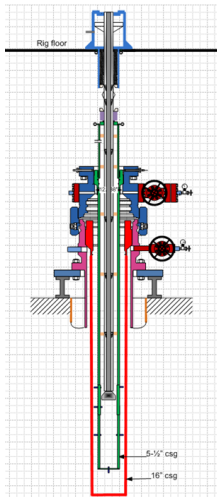
Assembly step 9:

Place drill rod. Drill string is supported by the top lid. Check the signal in the cable.

Place the drill string guide plate (bottom of nitrogen vessel). Bolt guide plate + spring kit in place to the base plate.

Place piston section.

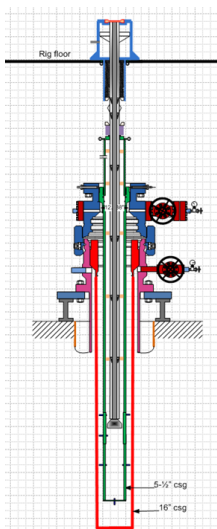
Figure B.3: Assembly step 7,8,9



Assembly step 10:
Place the top rod

Install casing around piston, including seals.

Install outer support pipe



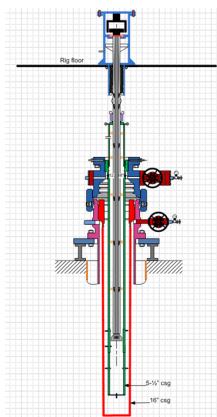
Assembly step 11:

Place shear pin above the drill string. Run wire through the break disc, leave enough cable inside casing (500mm).

Place intermediate plate outer support pipe and bolt together

Pressurize cylinder until rod runs into shear pin (pressure about 10 bar).

Check the signal in cable and guide the cable.

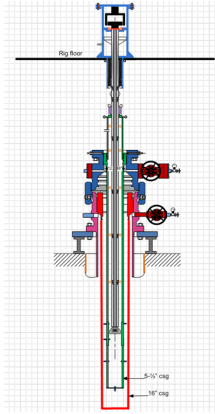


Assembly step 12:

Install the damper above the shear pin. Connect accelerometer wiring at the top, leave enough cable inside casing (500mm). Install the protective casing. Check the signals in all cables.

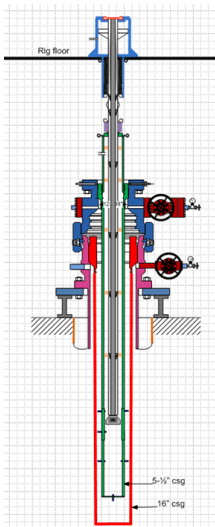
Figure B.4: Assembly step 10,11,12

B.2. shear pin change



Shear pin change step 1:

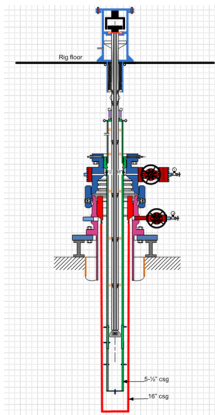
Equilibrium between gas pressure and spring force. Depressurize water vessel. Depressurize nitrogen vessel until bulge rests on top lid.



Shear pin change step 2: Remove top casing and damper, remove intermediate plate. Check wiring. Remove old shear pin. Place new shear pin. Place intermediate plate outer support pipe and bolt together.

Pressurize cylinder until rod runs into shear pin (pressure about 10 bar).

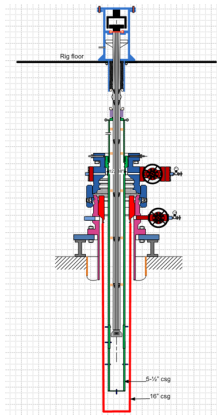
Check the signal in cable and guide the cable.



Shear pin change step 3: Install the damper above the breakdisc. Connect accelerometer wiring at the top, leave enough cable inside casing (500mm). Install protective casing.

Figure B.5: shear pin change step 1,2,3

B.3. Cone change

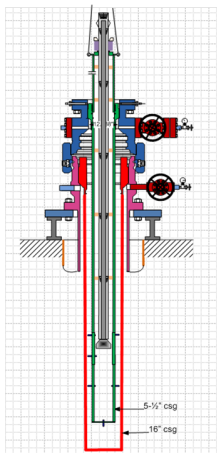


Cone change step 1: Equilibrium between gas pressure and spring force. Depressurize water vessel. Depressurize nitrogen vessel until bulge rests on top lid.

Remove complete top section. Unbolt centre plate from rig floor, keep outer plate in place because of centration.

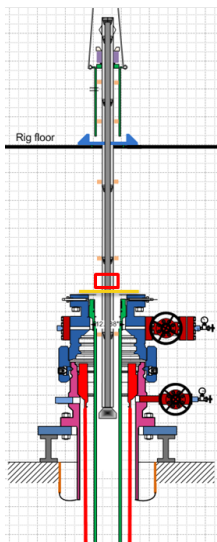
Lift complete top section so string can be broken between bulge and cover lid.

Place C-plate. Break the drill string. Move out of the way top section



Cone change step 2:

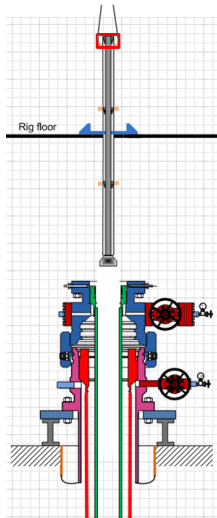
Disconnect top plate lid and lift together with drill string to maximum height.



Cone change step 3:

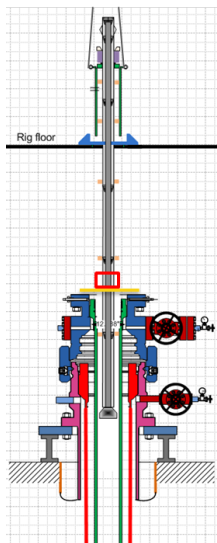
Place C-plate on top of hanger and install lift clamp to hang-off on top of hanger. Disconnect top half and bottom half of drill string. Remove top-half of the drill string.

Figure B.6: Cone change step 1,2,3



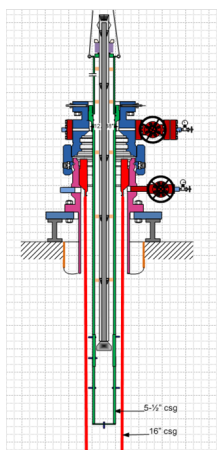
Cone change step 4:

Connect lifting clamp to bottom section of string. Lift until cone is out of well-head. Replace cones and reconnect wiring. Check signal.



Cone change step 5:

Place C-Plate, hang off bottom half drill string on C-plate. Lift and make-up top section of drill string. Top section is hanging on bulge (donut).



Cone change step 6:

Lower the top part of string fully to connect top plate lid.

Move in topsection

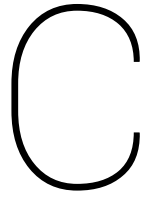
Reconnect the drill string

Lower topsection until centre plate is in place

Bolt centre plate to rig floor

Replace shear pin and continue with step 11 of assembly.

Figure B.7: Cone change step 4,5,6



FEA results by 4RealSim

During the design of the drill string, finite element analyses have been performed in order to determine forces on crucial positions in the design. On the next page the results are displayed that were used for the detailing of the experiment set-up. The input parameters are displayed in table C.1.

The following steps were performed:

Step 1 (static)

- Fix top of drill string axially
- Apply pressure on bottom of piston, total force = 361 [kN]

Step 2 (dynamic)

- Release top of drill string
- Pressure at bottom of piston: $P = P_0 \cdot (V/V_0)^{-\gamma}$, $\gamma = 1.4$
- P_0 is pressure at end of step 1
- V_0 is volume of column of 800[mm] high
- V is calculated from piston displacement during step 2

Table C.1: FEA input variables

Variable	value	unit
Piston		
ρ	4500	$[kg/m^3]$
E	116	[GPa]
M	8	[kg]
Drill string		
ρ	7850	$[kg/m^3]$
E	210	[GPa]
Damper		
ρ (scaled to get correct mass)	15213	$[kg/m^3]$
E	230	[GPa]
M	22.1	[kg]
c_{damper}	11050	$N(s/m)^2$
Cone		
M	11.25	[kg]
Spring with 100mm play		
M	30	[kg]
k_{spring}	1.06e+4	[-]

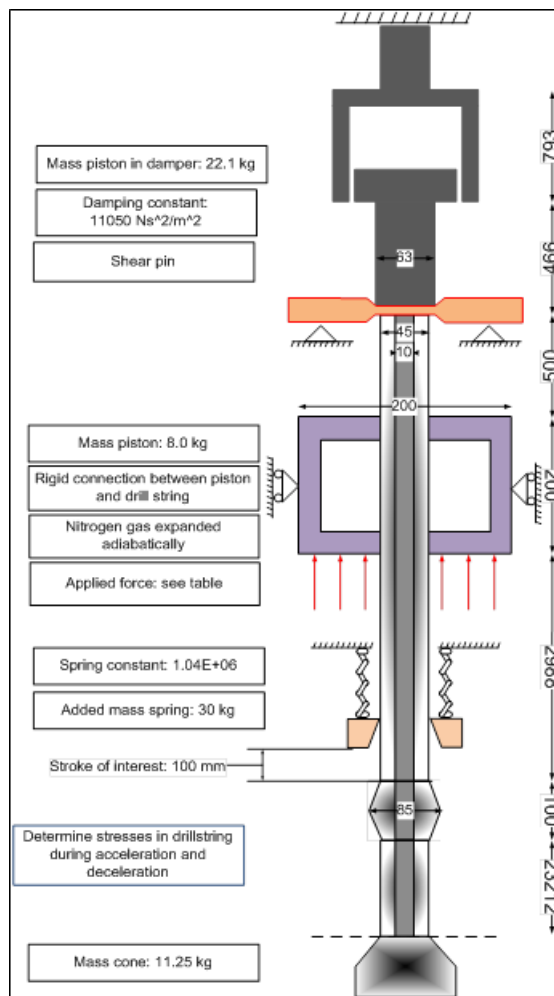


Figure C.1: Schematic overview of the FEA input

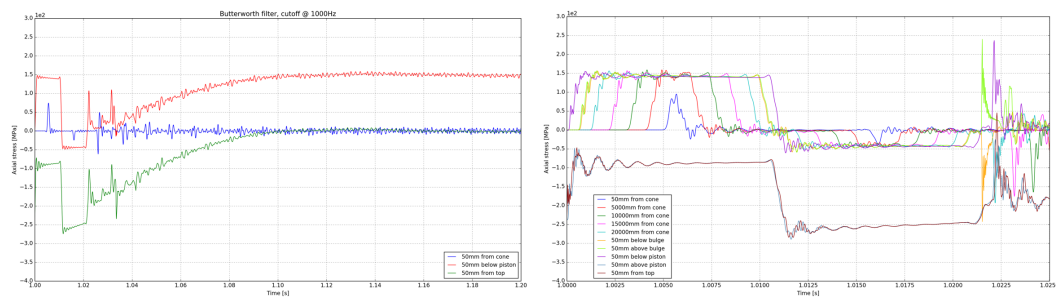


Figure C.2: Axial stresses at release (left) and until the bulge hits the spring (right)

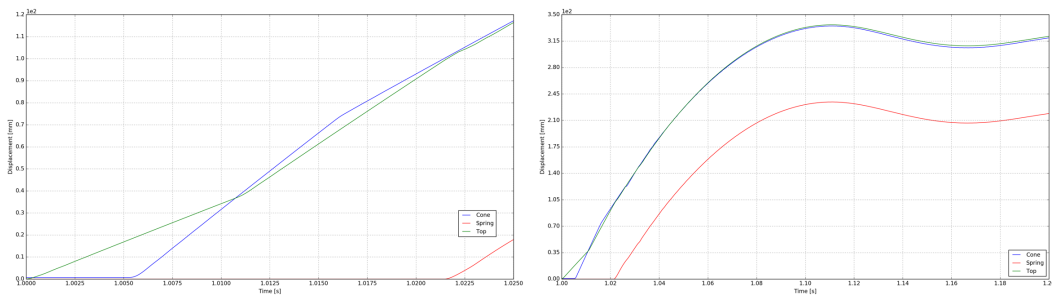


Figure C.3: Displacements of the cone, spring and top of the drill string during stroke of interest (left) and including deceleration of the system (right)

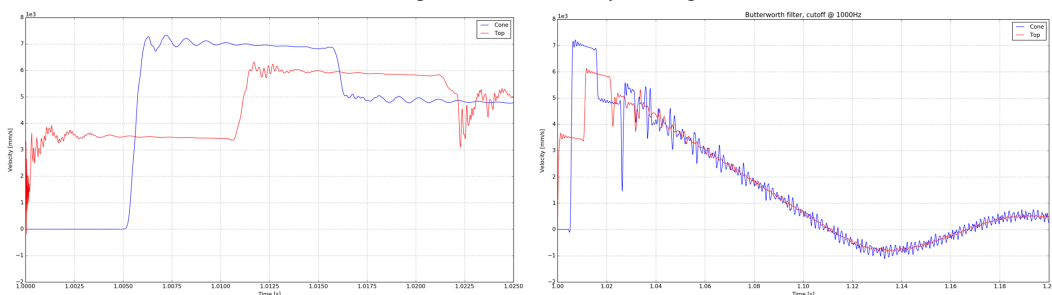


Figure C.4: Displacements of the cone, spring and top of the drill string during stroke of interest (left) and including deceleration of the system (right)

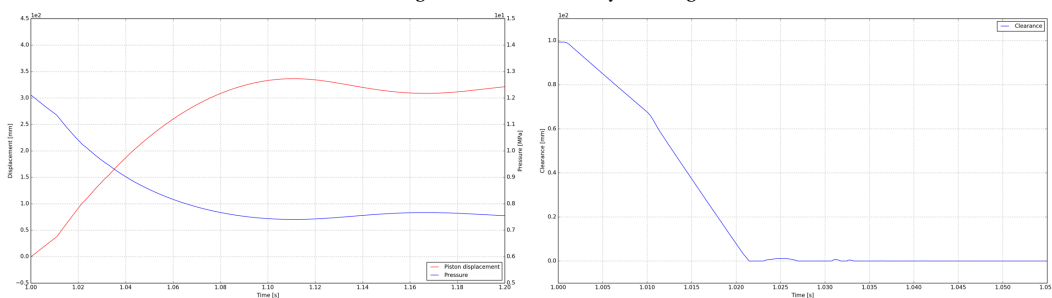


Figure C.5: Piston displacement and pressure in vessel (left) and the clearance between bulge and friction spring (right)

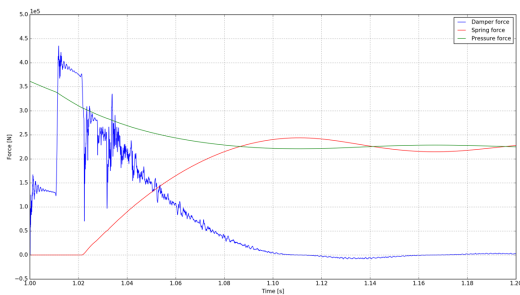
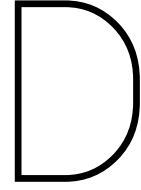


Figure C.6: Forces in the damper, spring and nitrogen vessel



Derivation of Bernoulli's equation for unsteady flow

In this appendix, the full derivation of Bernoulli's equation for unsteady flow is given, using Battjes' Korte Golven (1986)[13]. It is assumed that the velocity field is free from rotation, and can be derived from a scalar field. The velocity-potential then becomes:

$$\vec{u} = \nabla\phi \quad (\text{D.1})$$

Thereby:

$$u = \frac{\partial\phi}{\partial x}, v = \frac{\partial\phi}{\partial y}, w = \frac{\partial\phi}{\partial z} \quad (\text{D.2})$$

Since we assume an incompressible fluid:

$$\nabla \times \vec{u} = 0 \Rightarrow \nabla \times \nabla\phi = 0 \Rightarrow \nabla^2\phi = 0 \quad (\text{D.3})$$

Rewritten as Laplace's equation:

$$\frac{\partial^2\phi}{\partial^2x} + \frac{\partial^2\phi}{\partial^2y} + \frac{\partial^2\phi}{\partial^2z} = 0 \quad (\text{D.4})$$

When assuming incompressibility, the Bulk modulus reaches infinity ($K \rightarrow \infty$) and thereby also the propagation speed of the wave ($c = \sqrt{\frac{K}{\rho}}$). This means that in the area where this equation is used, all relations are calculated without time delay.

Using the Navier-Stokes equation:

$$\frac{D\vec{u}}{Dt} = \vec{g} - \frac{1}{\rho}\nabla p + \nu\nabla^2\vec{u} \quad (\text{D.5})$$

Where the following parts can be rewritten:

$$\frac{D}{Dt} = \frac{\partial}{\partial t} + \vec{u}\nabla \quad (\text{D.6})$$

$$\vec{g} = -\nabla(gz) \quad (\text{D.7})$$

When the density, ρ is assumed constant the terms $\vec{g} - \frac{1}{\rho}\nabla p$ can be rewritten as $-\nabla(\frac{p}{\rho} + gz)$ and the formula reduces to:

$$\frac{\partial\vec{u}}{\partial t} + (\vec{u} \cdot \nabla)\vec{u} = -\nabla(\frac{p}{\rho} + gz) + \nu\nabla^2\vec{u} \quad (\text{D.8})$$

The last term is the viscosity term and when assuming rotation-free ($\vec{u} = \nabla\phi$) and incompressibility ($\nabla^2\phi = 0$) it is reduced to:

$$\nu\nabla^2(\nabla\phi) = \nu\nabla(\nabla^2\phi) = \nu\nabla(0) = 0 \quad (\text{D.9})$$

The first term can be reduced as:

$$\frac{\partial \vec{u}}{\partial t} = \frac{\partial}{\partial t}(\nabla\phi) = \nabla\left(\frac{\partial\phi}{\partial t}\right) \quad (\text{D.10})$$

The term $(\vec{u}\nabla)u$, considering 1 directional component (take the x-component) is rewritten as:

$$(\vec{u}\cdot\nabla)u = u\frac{\partial u}{\partial x} + v\frac{\partial v}{\partial y} + w\frac{\partial w}{\partial z} \quad (\text{D.11})$$

The rotational components are assumed 0 ($\frac{\partial u}{\partial y} = \frac{\partial v}{\partial x}$, etc., therefore:

$$(\vec{u}\cdot\nabla)u = u\frac{\partial u}{\partial x} + v\frac{\partial v}{\partial x} + w\frac{\partial w}{\partial x} \quad (\text{D.12})$$

And:

$$(\vec{u}\cdot\nabla)u = \frac{\partial}{\partial x}\left(\frac{1}{2}u^2 + \frac{1}{2}v^2 + \frac{1}{2}w^2\right) = \frac{\partial}{\partial x}\left(\frac{1}{2}|\vec{u}|^2\right) = \frac{\partial}{\partial x}\left(\frac{1}{2}|\nabla\phi|^2\right) \quad (\text{D.13})$$

So that for each direction the term has a value of, for x: $\frac{\partial}{\partial x}\left(\frac{1}{2}|\vec{u}|^2\right)$, for y: $\frac{\partial}{\partial y}\left(\frac{1}{2}|\vec{u}|^2\right)$, for z: $\frac{\partial}{\partial z}\left(\frac{1}{2}|\vec{u}|^2\right)$. For the total term $(\vec{u}\cdot\nabla)\vec{u}$ it will be:

$$(\vec{u}\cdot\nabla)\vec{u} = \nabla\left(\frac{1}{2}|\vec{u}|^2\right) = \nabla\left(\frac{1}{2}|\nabla\phi|^2\right) \quad (\text{D.14})$$

Using equations D.9, D.10, D.13, and D.14, and substituting them in equation D.8 gives:

$$\nabla\left(\frac{\partial\phi}{\partial t} + \frac{1}{2}|\nabla\phi|^2 + \frac{p}{\rho} + gz\right) = 0 \quad (\text{D.15})$$

This is the equation used for the coupling discussed in chapter 4.